Published November 14, 2011

We found no engraftment in both mice (Fig. 7 L), which indicates that the resistance to the donor HSC engraftment during steady-state hematopoiesis is maintained in *Evi1*$^{+/-}$ mice. Collectively, these data suggest that Evi1 is dispensable for the regulation of proliferative and differentiation capacity of ST-HSCs/MPPs, but is strictly required for the maintenance of LT-HSC activity.

To investigate the mechanism behind the impaired HSC activity, we performed cell-cycle and apoptosis assays, but found no differences in the cell-cycle profile or apoptotic rates of Flk-2$^-$ CD34$^-$ LSK cells between *Evi1*$^{+/+}$ and *Evi1*$^{+/-}$ mice (unpublished data). Collectively, in consideration of the accelerated loss of LT-HSC activity in *Evi1*$^{+/-}$ mice, it is supposed that Evi1 heterozygosity directs LT-HSCs from self-renewal toward differentiation to generate more committed progenitors, which is uncoupled from cell-cycle progression or apoptosis.

Forced expression of Evi1 prevents HSPC differentiation and enhances their expansion

The findings noted above led us to hypothesize Evi1 has the potential to inhibit differentiation and enhance HSC self-renewal independent of cell-cycle progression. To clarify this, we adopted a gain-of-function approach, in which WT LSK cells were transduced with Evi1, and then incubated in serum-free medium. Although forced expression of Evi1 gave no apparent growth advantage for the first 10 d of culture, Evi1-transduced LSK cells subsequently manifested a mild but significant increase in proliferation rate (Fig. 8 A). Moreover, we found a substantial increase in the frequency of the remaining LSK fraction in cultured Evi1-transduced cells compared with control cells (Fig. 8 B). In parallel, the number of colonies derived from cultured Evi1-transduced LSK cell was drastically increased (Fig. 8 C). These results suggest that Evi1 activation restricts lineage differentiation and enhances self-renewal activity of HSPCs. Collectively, our data provide compelling evidence that Evi1 regulates the developmental transition from HSPCs to more committed progenitors, suggesting a crucial role of Evi1 in controlling the balance between self-renewal and differentiation.

A recent work suggests that the longer, PR domain-containing isoform Mds1-Evi1 (ME) deficiency alone causes a reduction in the number of HSCs with a loss of long-term repopulation capacity (Zhang et al., 2011). Because both ME and Evi1 are inactivated in our *Evi1* KO model (Goyama et al., 2008), we attempted to genetically dissect the relative roles of ME and Evi1 in maintaining LT-HSCs. For this purpose, we transduced Evi1 or ME into *Evi1*$^{+/-}$ Flk-2$^-$ CD34$^-$ LSK cells and examined whether they could maintain stem cell phenotype after in vitro culture. Reintroduction of Evi1 led to a significant increase in the proportion that remained in the LSK fraction, similar to observations made in *Evi1*$^{+/+}$ cells (Fig. 8 D). However, retroviral transfer of ME was unable to normalize the frequency of the remaining LSK fraction (Fig. 8 D), indicating that Evi1 preferentially rescues *Evi1*$^{+/-}$ LT-HSC defects. Given that ME has broader effects on the hematopoietic system than Evi1 and acts in part by maintaining HSC quiescence through up-regulation of *Cdkn1c* transcription (Zhang et al., 2011), Evi1 and ME may exert their functions in regulating hematopoiesis at different stages and by different mechanisms.

DISCUSSION

In this study, we show that the amount of *Evi1* transcript can be indicative of an undifferentiated state with multipotent differentiation capacity within HSPCs. In both the fetal and adult hematopoietic systems, Evi1 expression can mark long-term multilineage repopulating HSCs, and enhance HSC purification with a combination of other surface markers, suggesting a specific relationship between HSC activity and Evi1 expression throughout ontogeny. This stem cell-specific expression pattern of Evi1 allows us to functionally identify self-renewing HSCs by using Evi1-IRES-GFP knock-in mice, and suggests the relevance of Evi1 in fine-tuning of stem cell properties. Indeed, we provide the genetic evidence confirming that Evi1 has a predominant effect on LT-HSCs by specifically regulating their self-renewal capacity.

The prospective isolation of HSCs is the most important step to dissect their function. The strategy commonly used for HSC isolation is purification based on the expression of a combination of cell surface markers. However, some of these parameters differ between strains of mice, change dramatically during development, and are expressed on many non-HSCs.

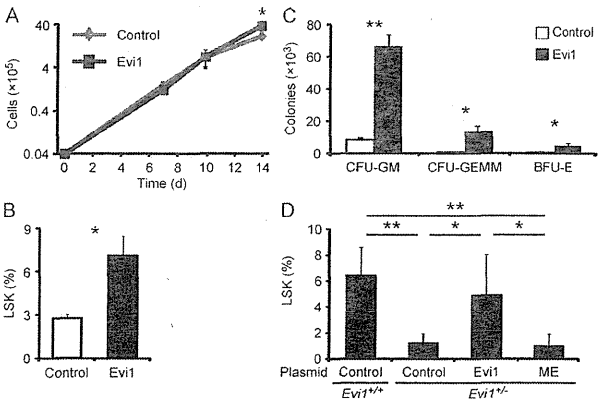

Figure 8. Forced expression of Evi1 prevents HSPC differentiation and promotes their expansion. (A) Proliferation of 3,000 control- or Evi1-transduced LSK cells cultured in serum-free medium with 20 ng/ml SCF and 20 ng/ml TPO for 14 d (*, $P < 0.05$; $n = 3$). (B) After 7 d of culture, the percentage of the remaining LSK fraction in cultured control- or Evi1-transduced LSK cells was analyzed (*, $P < 0.01$; $n = 3$). (C) In vitro colony-forming assay was performed to assess the numbers of CFU-GM, CFU-GEMM, and BFU-E colonies after 3,000 control- or Evi1-transduced LSK cells were cultured for 14 d (*, $P < 0.005$; **, $P < 0.0005$; $n = 3$). (D) Control-, Evi1-, or ME-transduced *Evi1*$^{+/+}$ or *Evi1*$^{+/-}$ Flk-2$^-$ CD34$^-$ LSK cells were cultured in medium containing 10% serum with 50 ng/ml SCF, 50 ng/ml TPO, 10 ng/ml IL-3, and 10 ng/ml IL-6 for 5 d, and the percentages of the remaining LSK fraction were analyzed (*, $P < 0.05$; **, $P < 0.0005$; $n = 5$–6). Data represent mean ± SD.

Published November 14, 2011

Here, we reveal that Evi1 expression specifically correlates with functional HSCs, whereas lack of Evi1 expression exclusively identifies cells without functional HSC activity in both the fetal and adult hematopoietic systems. In particular, Evi1 expression can segregate long-term repopulating HSCs from cells without self-renewal potential even within the highly subfractionated Flk-2$^-$ CD34$^-$ LSK or CD48$^-$ CD150$^+$ LSK compartments. In addition, Evi1-IRES-GFP knock-in mice offer advantages over the conventional HSC surface markers, as the GFP$^-$ and GFP$^+$ subfractions of the Flk-2$^-$ CD34$^-$ LSK or CD48$^-$ CD150$^+$ LSK cells show a quite similar distribution of these markers (unpublished data). Moreover, our findings that Evi1 specifically regulates the self-renewal capacity of HSCs guarantee the potential utility of Evi1 expression as an indicator of HSC activity. Therefore, the Evi1-IRES-GFP knock-in mouse line provides a powerful approach for the functional identification of self-renewing HSCs in vivo, thus opening a new avenue for investigating HSC biology.

Although functional HSCs exclusively reside in the GFP$^+$ population, a proportion of GFP$^+$ cells lack HSC function. As GFP protein is quite stable and degraded more slowly than Evi1 protein (unpublished data), these observations may reflect a remnant of GFP expression from cells that have just differentiated from GFP$^+$ HSCs. However, it is possible that Evi1 expression distinguishes self-renewing ST-HSCs from cells with no self-renewal activity in the ST-HSC/MPP fraction, as Evi1 heterozygosity affects the short-term repopulating capacity of CD34$^+$ LSK cells.

The present findings in the hematopoietic system encourage us to examine the possibility that Evi1 expression serves as a selective marker for stem cells in other tissues or in cancer systems. We show that mesenchymal stem cells (MSCs), one of the few tissue stem cell types that have been established to self-renew in vivo (Morikawa et al., 2009), do not express Evi1. However, a mouse gene expression atlas and prior studies examining the expression pattern of Evi1 in various tissues have reported Evi1 expression in the kidney, ovary, uterus, intestine, stomach, lung, trachea, and nasal cavity in the adult mouse (Morishita et al., 1990; Perkins et al., 1991; Su et al., 2004). It will be interesting to determine, using Evi1-IRES-GFP knock-in mice, whether Evi1-expressing cells in these organs are enriched with tissue stem cells.

Our data suggest a unique association between Evi1 expression and HSC self-renewal activity throughout hematopoietic ontogeny. Along with this stem cell–specific expression pattern of Evi1, the fact that the disruption of a single allele of Evi1 leads to a near total loss of self-renewing HSCs implicates Evi1 as a central regulator in HSC self-renewal. In addition, a recent gene expression profile analysis showed that Evi1 binding sites are enriched in the upstream region of genes expressed selectively in LT-HSCs (Forsberg et al., 2010). In fact, several molecules involved in the regulation of HSC self-renewal have been identified as downstream targets or interacting proteins of Evi1, including Gata2 (Sato et al., 2008; Yuasa et al., 2005), Pbx1 (Shimabe et al., 2009), Runx1 (Senyuk et al., 2007), and TGF-β (Kurokawa et al., 1998). Together with these findings, our data strongly support a model in which Evi1 gene dosage is a critical determinant of HSC self-renewal potential.

Inappropriate expression of EVI1 confers poor prognosis in patients with AML (Lugthart et al., 2008; Gröschel et al., 2010), and therefore improvement of the therapeutic outcome of leukemia with high EVI1 expression is needed. In this study, we reveal that Evi1 overexpression blocks differentiation and induces HSPC expansion. Our data fit with other studies showing that retroviral integration at the *Evi1* locus can be associated with long-term in vivo clonal dominance, occasionally leading to leukemic transformation (Stein et al., 2010). The genetic events underlying AML pathogenesis fall into two groups: (1) mutations that enhance proliferation and survival of hematopoietic progenitors, or (2) mutations that result in impaired differentiation or aberrant acquisition of self-renewal properties of HSPCs (Fröhling et al., 2005). Our data indicate that Evi1 activation can function as the latter mutation and confer enhanced self-renewal capacity in myeloid neoplasms. In addition, we demonstrate that retroviral transfer of Evi1, but not ME, can ameliorate the self-renewal defects in *Evi1*$^{+/-}$ HSCs, highlighting a distinct role of Evi1 in HSC self-renewal. These findings may explain the underlying mechanisms of the clinical observations that, irrespective of ME expression, aberrant EVI1 expression carries an adverse prognostic value in AML (Lugthart et al., 2008, 2010). As it is becoming evident that leukemic stem cells share self-renewal machinery with normal HSCs, the elucidation of how Evi1 controls HSC self-renewal may provide biological insight into the pathogenesis of Evi1-related leukemia.

MATERIALS AND METHODS

Generation of Evi1-IRES-GFP knock-in mice. The targeting construct was assembled in the plasmid vector pBluescript KS. The 5′ arm of the targeting vector consists of a 5.1-kb fragment of BAC clone RP24-481A14 and the 3′ arm consists of a 3.1-kb fragment. The 5′ arm contains *Evi1* intron 8 and exon 9, and the 3′ arm contains intron 9, exon 10, and intron 10. Both arms were obtained by PCR using BAC clone RP24-481A14 as a template, all sequenced, and then inserted into pBluescript KS. Mouse *Evi1* cDNA was isolated from murine embryo cDNA by PCR, with an EcoRI site at the 5′ end and a BamHI site at the 3′ end, which was cloned into pBluescript KS. A 1.3-kb IRES-GFP cassette derived from pGCDNsam-IRES-GFP retroviral vector was inserted downstream of the aforementioned *Evi1* fragment. A polyadenylation (pA) cassette was then ligated 3′ to the IRES-GFP cassette. A neomycin-positive selection (Neo^r) cassette, expressed under control of the PGK promoter, was inserted downstream of the pA cassette. Both pA cassette and loxP-flanked neomycin-positive selection cassette were derived from DT-A/AFP(EGFP)/Neo vector (a gift from the Institute of Physical and Chemical Research Center for Developmental Biology, Kobe, Japan). The partial *Evi1 cDNA-IRES-GFP-pA-loxP-neo* was released intact by digestion with *Sse*8387I and cloned into a unique *Sse*8387I site in exon 9 of BAC arm. A diphtheria toxin–negative selection cassette was cloned into pBluescript KS, 3′ to the targeting construct. The targeting construct was linearized by SacII and transfected into TT2 ES cells by electroporation. Homologous recombinant clones were identified by Southern blot analysis of genomic DNA isolated from individual G418/FIAU-resistant ES cell colonies. The DNA was digested with XbaI, blotted to nylon membranes, and

Published November 14, 2011

JEM

hybridized with a 3′ external *Evi1* probe. Confirmatory Southern blotting could detect a 9.1-kb WT *Evi1* allele band and a 4.1-kb correctly targeted *Evi1-IRES-GFP* allele band with this 3′ probe. In EcoRV-digested genomic DNA from positive ES cell clones, a 5′ external probe detected 10- and 11-kb bands from the WT and targeted alleles, respectively. Next, appropriately targeted ES clones were aggregated with 8-cell stage of ICR embryo, and resultant blastocysts were injected into pseudopregnant foster ICR mothers. Chimeric males, which gave germ-line transmission, were crossed with C57BL/6 females. Blastocyst injection and breeding of chimeras were performed in the Animal Center for Biomedical Research, University of Tokyo, Tokyo, Japan.

Mice. Evi1-IRES-GFP knock-in mice were backcrossed onto a C57BL/6 background (Ly5.1 or Ly5.2) for at least four generations (Sankyo-Laboratory Service). Heterozygous *Evi1* KO mice ($Evi1^{+/-}$ mice) were previously described (Goyama et al., 2008). C57BL/6-Ly5.1 mice were crossed with Ly5.2 mice to obtain Ly5.1/Ly5.2 mice. Littermates were used as controls in all experiments. All animal experiments were approved by the University of Tokyo Ethics Committee for Animal Experiments and strictly adhered to the guidelines for animal experiments of the University of Tokyo.

Genotype analysis. $Evi1^{+/-}$ mice were genotyped by PCR as previously described (Goyama et al., 2008). $Evi1^{+/GFP}$ mice were genotyped using a multiplex PCR to detect both WT and *Evi1-IRES-GFP* alleles. Genomic DNA was isolated from tail biopsies and subjected to PCR using *Neo* and *Evi1* primers. PCR with *Neo* primers detects the knock-in allele, and that with *Evi1* primers detects the WT allele. The PCR samples were denatured at 94°C for 2 min, subjected to 30 cycles of amplification (94°C for 30 s, 65°C for 1 min, and 72°C for 1 min), and followed by a final extension step at 72°C. PCR products were resolved by agarose gel electrophoresis. PCR primers are listed below: *Neo* primer forward, 5′-AGGGGATCCGCTGTAAGTCT-3′, reverse, 5′-GCACTGACTGCTCATCCAAA-3′; *Evi1* primer forward, 5′-ATGTCAGCAATTGAGAACATGG-3′, reverse, 5′-ATCCAAAGGTCCTGAGTTCAAA-3′.

Flow cytometry. A list of antibodies is provided in Table S1. Stained cells were sorted with a FACSAriaII, and analysis was performed on LSRII (both from BD). A mixture of antibodies recognizing CD3, CD4, CD8, B220, TER-119, Mac-1, or Gr-1 was used to identify Lin^+ cells. Anti-CD127 antibody was added to the lineage mixture, except for the analysis of CLPs. The data analyses were performed with FlowJo software (Tree Star). In experiments with the Evi1-IRES-GFP knock-in mouse, a "fluorescence minus one" littermate control was analyzed in parallel to set GFP gates.

Cell-cycle analyses. For Hoechst 33342 and pyronin Y staining, cells were incubated with 5 ng/ml Hoechst 33342 (Invitrogen) and 25 µg/ml verapamil at 37°C for 45 min. Next, pyronin Y (Sigma-Aldrich) was added to 1 µg/ml, and the cells were incubated for an additional 15 min.

In vitro culture. For in vitro serum-free culture, cells were cultured in StemSpan SFEM (StemCell Technologies) supplemented with 20 ng/ml mouse SCF and 20 ng/ml human TPO, and subsequently subjected to flow cytometry or colony-forming assay at the indicated day after incubation. For colony-forming assay, cells were seeded in duplicate and cultured in cytokine-supplemented methylcellulose medium (MethoCult GF M3434; Stem Cell Technologies). Subsequently, colonies were counted and identified based on morphological examination on day 12. For in vitro differentiation, LSK GFP^+ cells were cultured in RPMI-1640 medium (Wako) containing 10% serum with 50 ng/ml mouse SCF, 50 ng/ml human TPO, 10 ng/ml mouse IL-3, and 10 ng/ml human IL-6, and subjected to flow cytometry or colony-forming assay after 5 d of incubation.

Single-cell culture. Cells were clone-sorted into 96-well plates using FACS-based automated cell deposition unit and cultured in StemSpan SFEM supplemented with 20 ng/ml mouse SCF and 20 ng/ml human TPO. After 14 d of culture, cell numbers in each colony were analyzed.

In vivo transplantation assay. Transplantation assays were performed using the Ly5 congenic mouse system. In CRAs, lethally irradiated (9.5 Gy) mice were reconstituted with the indicated subsets from $Evi1^{+/+}$, $Evi1^{+/GFP}$, or $Evi1^{+/-}$ mice, in competition with 2×10^5 unfractionated BM cells from congenic mice. For second BM transplantation, BM cells (1/2 femur equivalent) were obtained from recipient mice 16 wk after transplantation, and transplanted into a second set of lethally irradiated (9.5 Gy) mice. For reciprocal transplantation assays, lethally irradiated (9.5 Gy) or unirradiated $Evi1^{+/+}$ and $Evi1^{+/-}$ mice were transplanted with 2×10^5 WT BM cells without competitor cells. In non-CRAs, lethally irradiated (9.5 Gy) mice were reconstituted with $Evi1^{+/+}$ and $Evi1^{+/-}$ $Flk\text{-}2^-$ $CD34^-$ LSK cells without competitor cells. Reconstitution of donor-derived cells was monitored by staining PB cells with antibodies against Ly5.1, Ly5.2, CD3, CD4, CD8, B220, Mac-1, and Gr-1. When $CD48^+$ $CD150^-$ LSK cells were transplanted, nonblocking anti-CD48 antibody (MRC OX78 clone) was used (Grassinger et al., 2010).

CFU-S assay. For CFU-S assay, 100 $CD34^+$ LSK cells were injected into lethally irradiated (9.5 Gy) mice. Spleens in transplanted mice were isolated 11 d later, and visually inspected for the presence of macroscopic colonies after fixation in Tellyesniczky's solution.

RQ-PCR. Total RNA was prepared using RNeasy Mini kit (QIAGEN), then cDNA was synthesized with a QuantiTect Reverse Transcription kit (QIAGEN), and used for RQ-PCR with FastStart SYBR Green Master and LightCycler 480 System (Roche Applied Science) according to the manufacturer's instructions. All assays were performed in triplicate and relative expression was normalized to the internal control *GAPDH*. PCR primers are listed below: *GAPDH* primer forward, 5′-CCATCACCATCTTCCAGGAG-3′, reverse, 5′-CCTGCTTCACCACCTTCTTG-3′; *Evi1* primer forward, 5′-ATCGGAAGATCTTAGATGAGTTTTG-3′, reverse, 5′-CTTCCTACATCTGGTTGACTGG-3′

Western blotting. Western blotting was performed as previously described (Goyama et al., 2008). In brief, mouse embryo fibroblast cells were lysed in TNE buffer, subjected to 7% SDS-PAGE, and transferred to a PVDF membrane (Millipore). The blot was incubated with an Evi-1 (C50E12) rabbit monoclonal antibody (Cell Signaling Technology), and visualized by ECL Plus (GE Healthcare).

AGM and placental cell preparation. The day of vaginal plug observation was considered as day 0.5 postcoitum (E0.5). E10.5 AGM region or E12.5 placenta were carefully dissected from embryos, dissociated by incubation with 250 U/ml dispase (Godo Shusei) for 20 min and cell dissociation buffer (Invitrogen) for 20 min at 37°C, and followed by passages through 18–25 G needles. Single cell suspensions were filtered through 70-µm cell strainer and analyzed by flow cytometry.

Endothelial cell (EC), osteoblast (OB), and MSC preparation. After BM cells were flushed out, bones were crushed with a pestle and mortar. Then bone fragments were incubated with a Collagenase/Dispase (1 mg/ml; Roche Applied Science) in MEM α (Wako) with 20% serum and gently agitated for 90 min at 37°C. The dissociated cells were collected, and bone-associated mononuclear cells were isolated with the use of density centrifugation with Histopaque-1083 (Sigma-Aldrich). ECs were defined as $CD31^+$ $TER\text{-}119^-$ $CD45^-$, OBs were defined as $CD31^-$ $TER\text{-}119^-$ $CD45^-$ $Sca\text{-}1^-$ $ALCAM^+$ cells (Nakamura et al., 2010), and MSCs were defined as $CD31^-$ $TER\text{-}119^-$ $CD45^-$ $Sca\text{-}1^+$ $PDGFR\alpha^+$ cells (Morikawa et al., 2009).

Plasmid construct and retroviral transduction of LSK cells. The murine *Evi1* or *ME* cDNA were inserted into a site upstream of an IRES-EGFP cassette in the retroviral vector pGCDNsam. To produce Evi1-GFP–expressing retrovirus, Plat-E packaging cells were transiently transfected with retroviral constructs by using FuGENE 6 transfection reagent (Roche). LSK cells were purified and incubated in StemSpan SFEM medium and cytokines (100 ng/ml mouse SCF and 100 ng/ml human TPO) for 24 h.

Published November 14, 2011

Next, cultured LSK cells were infected with Evi1-GFP retrovirus in the presence of RetroNectin (Takara Bio Inc.). The infected LSK cells were harvested 36 h after retrovirus infection, and GFP$^+$ cells were sorted and subjected to in vitro culture. For retroviral transduction of Evi1 or ME into *Evi1*$^{+/+}$ and *Evi1*$^{+/-}$ Flk-2$^-$ CD34$^-$ LSK cells, those cells were sorted and immediately infected with Evi1- or ME-GFP retroviruses in the presence of RetroNectin. These cells were incubated in RPMI-1640 medium containing 10% serum and cytokines (50 ng/ml mouse SCF, 50 ng/ml human TPO, 10 ng/ml mouse IL-3, and 10 ng/ml human IL-6). After 5 d of culture, the percentage of the remaining LSK fraction in GFP$^+$ cells was analyzed by flow cytometry.

Statistical analysis. Statistical significance of differences between parameters was assessed using a two-tailed unpaired Student's *t* test or Wilcoxon rank sum test.

Online supplemental material. Fig. S1 shows FACS gating strategy used to identify GFP$^+$ population from adult BM of *Evi1*$^{+/GFP}$ mice. Fig. S2 shows FACS gating strategy used to identify GFP$^+$ population from E12.5 placenta or E14.5 FL of *Evi1*$^{+/GFP}$ embryos. Table S1 lists the antibodies used for flow cytometry. Online supplemental material is available at http://www.jem.org/cgi/content/full/jem.20110447/DC1.

We thank T. Kitamura for Plat-E packaging cells; H. Nakauchi and M. Onodera for pGCDNsam-IRES-EGFP retroviral vector; Y. Shimamura, Y. Sawamoto, R. Takizawa, and Y. Oikawa for expert technical assistance; and Institute of Physical and Chemical Research Center for Developmental Biology for DT-A/AFP(EGFP)/Neo plasmid.

This work was supported in part by a Grant-in-Aid for Scientific Research from the Japan Society for the Promotion of Science and by Health and Labour Sciences Research grants from the Ministry of Health, Labour and Welfare. K. Kataoka is a Research Fellow of the Japan Society for the Promotion of Science.

The authors have no conflicting financial interests.

Submitted: 1 March 2011
Accepted: 14 October 2011

REFERENCES

Akashi, K., X. He, J. Chen, H. Iwasaki, C. Niu, B. Steenhard, J. Zhang, J. Haug, and L. Li. 2003. Transcriptional accessibility for genes of multiple tissues and hematopoietic lineages is hierarchically controlled during early hematopoiesis. *Blood.* 101:383–389. http://dx.doi.org/10.1182/blood-2002-06-1780

Bowie, M.B., K.D. McKnight, D.G. Kent, L. McCaffrey, P.A. Hoodless, and C.J. Eaves. 2006. Hematopoietic stem cells proliferate until after birth and show a reversible phase-specific engraftment defect. *J. Clin. Invest.* 116:2808–2816. http://dx.doi.org/10.1172/JCI28310

Buonamici, S., D. Li, Y. Chi, R. Zhao, X. Wang, L. Brace, H. Ni, Y. Saunthararajah, and G. Nucifora. 2004. EVI1 induces myelodysplastic syndrome in mice. *J. Clin. Invest.* 114:713–719.

Chen, W., A.R. Kumar, W.A. Hudson, Q. Li, B. Wu, R.A. Staggs, E.A. Lund, T.N. Sam, and J.H. Kersey. 2008. Malignant transformation initiated by Mll-AF9: gene dosage and critical target cells. *Cancer Cell.* 13:432–440. http://dx.doi.org/10.1016/j.ccr.2008.03.005

Forsberg, E.C., E. Passegué, S.S. Prohaska, A.J. Wagers, M. Koeva, J.M. Stuart, and I.L. Weissman. 2010. Molecular signatures of quiescent, mobilized and leukemia-initiating hematopoietic stem cells. *PLoS ONE.* 5:e8785. http://dx.doi.org/10.1371/journal.pone.0008785

Fröhling, S., C. Scholl, D.G. Gilliland, and R.L. Levine. 2005. Genetics of myeloid malignancies: pathogenetic and clinical implications. *J. Clin. Oncol.* 23:6285–6295. http://dx.doi.org/10.1200/JCO.2005.05.010

Goyama, S., and M. Kurokawa. 2009. Pathogenetic significance of ecotropic viral integration site-1 in hematological malignancies. *Cancer Sci.* 100:990–995. http://dx.doi.org/10.1111/j.1349-7006.2009.01152.x

Goyama, S., G. Yamamoto, M. Shimabe, T. Sato, M. Ichikawa, S. Ogawa, S. Chiba, and M. Kurokawa. 2008. Evi-1 is a critical regulator for hematopoietic stem cells and transformed leukemic cells. *Cell Stem Cell.* 3:207–220. http://dx.doi.org/10.1016/j.stem.2008.06.002

Grassinger, J., D.N. Haylock, B. Williams, G.H. Olsen, and S.K. Nilsson. 2010. Phenotypically identical hemopoietic stem cells isolated from different regions of bone marrow have different biologic potential. *Blood.* 116:3185–3196. http://dx.doi.org/10.1182/blood-2009-12-260703

Gröschel, S., S. Lugthart, R.F. Schlenk, P.J. Valk, K. Eiwen, C. Goudswaard, W.J. van Putten, S. Kayser, L.F. Verdonck, M. Lübbert, et al. 2010. High EVI1 expression predicts outcome in younger adult patients with acute myeloid leukemia and is associated with distinct cytogenetic abnormalities. *J. Clin. Oncol.* 28:2101–2107. http://dx.doi.org/10.1200/JCO.2009.26.0646

Kiel, M.J., O.H. Yilmaz, T. Iwashita, O.H. Yilmaz, C. Terhorst, and S.J. Morrison. 2005. SLAM family receptors distinguish hematopoietic stem and progenitor cells and reveal endothelial niches for stem cells. *Cell.* 121:1109–1121. http://dx.doi.org/10.1016/j.cell.2005.05.026

Kim, I., S. He, O.H. Yilmaz, M.J. Kiel, and S.J. Morrison. 2006. Enhanced purification of fetal liver hematopoietic stem cells using SLAM family receptors. *Blood.* 108:737–744. http://dx.doi.org/10.1182/blood-2005-10-4135

Kurokawa, M., K. Mitani, K. Irie, T. Matsuyama, T. Takahashi, S. Chiba, Y. Yazaki, K. Matsumoto, and H. Hirai. 1998. The oncoprotein Evi-1 represses TGF-beta signalling by inhibiting Smad3. *Nature.* 394:92–96. http://dx.doi.org/10.1038/27945

Lugthart, S., E. van Drunen, Y. van Norden, A. van Hoven, C.A. Erpelinck, P.J. Valk, H.B. Beverloo, B. Löwenberg, and R. Delwel. 2008. High EVI1 levels predict adverse outcome in acute myeloid leukemia: prevalence of EVI1 overexpression and chromosome 3q26 abnormalities underestimated. *Blood.* 111:4329–4337. http://dx.doi.org/10.1182/blood-2007-10-119230

Lugthart, S., S. Gröschel, H.B. Beverloo, S. Kayser, P.J. Valk, S.L. van Zelderen-Bhola, G. Jan Ossenkoppele, E. Vellenga, E. van den Berg-de Ruiter, U. Schanz, et al. 2010. Clinical, molecular, and prognostic significance of WHO type inv(3)(q21q26.2)/t(3;3)(q21;q26.2) and various other 3q abnormalities in acute myeloid leukemia. *J. Clin. Oncol.* 28:3890–3898. http://dx.doi.org/10.1200/JCO.2010.29.2771

McKinney-Freeman, S.L., O. Naveiras, F. Yates, S. Loewer, M. Philitas, M. Curran, P.J. Park, and G.Q. Daley. 2009. Surface antigen phenotypes of hematopoietic stem cells from embryos and murine embryonic stem cells. *Blood.* 114:268–278. http://dx.doi.org/10.1182/blood-2008-12-193888

Mikkola, H.K., and S.H. Orkin. 2006. The journey of developing hematopoietic stem cells. *Development.* 133:3733–3744. http://dx.doi.org/10.1242/dev.02568

Morikawa, S., Y. Mabuchi, Y. Kubota, Y. Nagai, K. Niibe, E. Hiratsu, S. Suzuki, C. Miyauchi-Hara, N. Nagoshi, T. Sunabori, et al. 2009. Prospective identification, isolation, and systemic transplantation of multipotent mesenchymal stem cells in murine bone marrow. *J. Exp. Med.* 206:2483–2496. http://dx.doi.org/10.1084/jem.20091046

Morishita, K., E. Parganas, D.M. Parham, T. Matsugi, and J.N. Ihle. 1990. The Evi-1 zinc finger myeloid transforming gene is normally expressed in the kidney and in developing oocytes. *Oncogene.* 5:1419–1423.

Nakamura, Y., F. Arai, H. Iwasaki, K. Hosokawa, I. Kobayashi, Y. Gomei, Y. Matsumoto, H. Yoshihara, and T. Suda. 2010. Isolation and characterization of endosteal niche cell populations that regulate hematopoietic stem cells. *Blood.* 116:1422–1432. http://dx.doi.org/10.1182/blood-2009-08-239194

Orford, K.W., and D.T. Scadden. 2008. Deconstructing stem cell self-renewal: genetic insights into cell-cycle regulation. *Nat. Rev. Genet.* 9:115–128. http://dx.doi.org/10.1038/nrg2269

Orkin, S.H., and L.I. Zon. 2008. Hematopoiesis: an evolving paradigm for stem cell biology. *Cell.* 132:631–644. http://dx.doi.org/10.1016/j.cell.2008.01.025

Perkins, A.S., J.A. Mercer, N.A. Jenkins, and N.G. Copeland. 1991. Patterns of Evi-1 expression in embryonic and adult tissues suggest that Evi-1 plays an important regulatory role in mouse development. *Development.* 111:479–487.

Ramalho-Santos, M., S. Yoon, Y. Matsuzaki, R.C. Mulligan, and D.A. Melton. 2002. "Stemness": transcriptional profiling of embryonic and adult stem cells. *Science.* 298:597–600. http://dx.doi.org/10.1126/science.1072530

Sato, T., S. Goyama, E. Nitta, M. Takeshita, M. Yoshimi, M. Nakagawa, M. Kawazu, M. Ichikawa, and M. Kurokawa. 2008. Evi-1 promotes

Published November 14, 2011

JEM

para-aortic splanchnopleural hematopoiesis through up-regulation of GATA-2 and repression of TGF-b signaling. *Cancer Sci.* 99:1407–1413. http://dx.doi.org/10.1111/j.1349-7006.2008.00842.x

Senyuk, V., K.K. Sinha, D. Li, C.R. Rinaldi, S. Yanamandra, and G. Nucifora. 2007. Repression of RUNX1 activity by EVI1: a new role of EVI1 in leukemogenesis. *Cancer Res.* 67:5658–5666. http://dx.doi.org/10.1158/0008-5472.CAN-06-3962

Shimabe, M., S. Goyama, N. Watanabe-Okochi, A. Yoshimi, M. Ichikawa, Y. Imai, and M. Kurokawa. 2009. Pbx1 is a downstream target of Evi-1 in hematopoietic stem/progenitors and leukemic cells. *Oncogene.* 28:4364–4374. http://dx.doi.org/10.1038/onc.2009.288

Stein, S., M.G. Ott, S. Schultze-Strasser, A. Jauch, B. Burwinkel, A. Kinner, M. Schmidt, A. Krämer, J. Schwäble, H. Glimm, et al. 2010. Genomic instability and myelodysplasia with monosomy 7 consequent to EVI1 activation after gene therapy for chronic granulomatous disease. *Nat. Med.* 16:198–204. http://dx.doi.org/10.1038/nm.2088

Su, A.I., T. Wiltshire, S. Batalov, H. Lapp, K.A. Ching, D. Block, J. Zhang, R. Soden, M. Hayakawa, G. Kreiman, et al. 2004. A gene atlas of the mouse and human protein-encoding transcriptomes. *Proc. Natl. Acad. Sci. USA.* 101:6062–6067. http://dx.doi.org/10.1073/pnas.0400782101

Takakura, N., T. Watanabe, S. Suenobu, Y. Yamada, T. Noda, Y. Ito, M. Satake, and T. Suda. 2000. A role for hematopoietic stem cells in promoting angiogenesis. *Cell.* 102:199–209. http://dx.doi.org/10.1016/S0092-8674(00)00025-8

Weksberg, D.C., S.M. Chambers, N.C. Boles, and M.A. Goodell. 2008. CD150- side population cells represent a functionally distinct population of long-term hematopoietic stem cells. *Blood.* 111:2444–2451. http://dx.doi.org/10.1182/blood-2007-09-115006

Yuasa, H., Y. Oike, A. Iwama, I. Nishikata, D. Sugiyama, A. Perkins, M.L. Mucenski, T. Suda, and K. Morishita. 2005. Oncogenic transcription factor Evi1 regulates hematopoietic stem cell proliferation through GATA-2 expression. *EMBO J.* 24:1976–1987. http://dx.doi.org/10.1038/sj.emboj.7600679

Zhang, Y., S. Stehling-Sun, K. Lezon-Geyda, S.C. Juneja, L. Coillard, G. Chatterjee, C.A. Wuertzer, F. Camargo, and A.S. Perkins. 2011. PR domain-containing Mds1-Evi1 is critical for long-term hematopoietic stem cells function. *Blood.* 118:3856–3861.

SnapShot: Insulin Signaling Pathways

Takashi Kadowaki, Kohjiro Ueki, Toshimasa Yamauchi, and Naoto Kubota
Department of Diabetes and Metabolic Diseases, Graduate School of Medicine, University of Tokyo,
Bunkyo-ku, Tokyo 113-8655, Japan

Insulin signaling through IRSs/PI3Ks/Akts

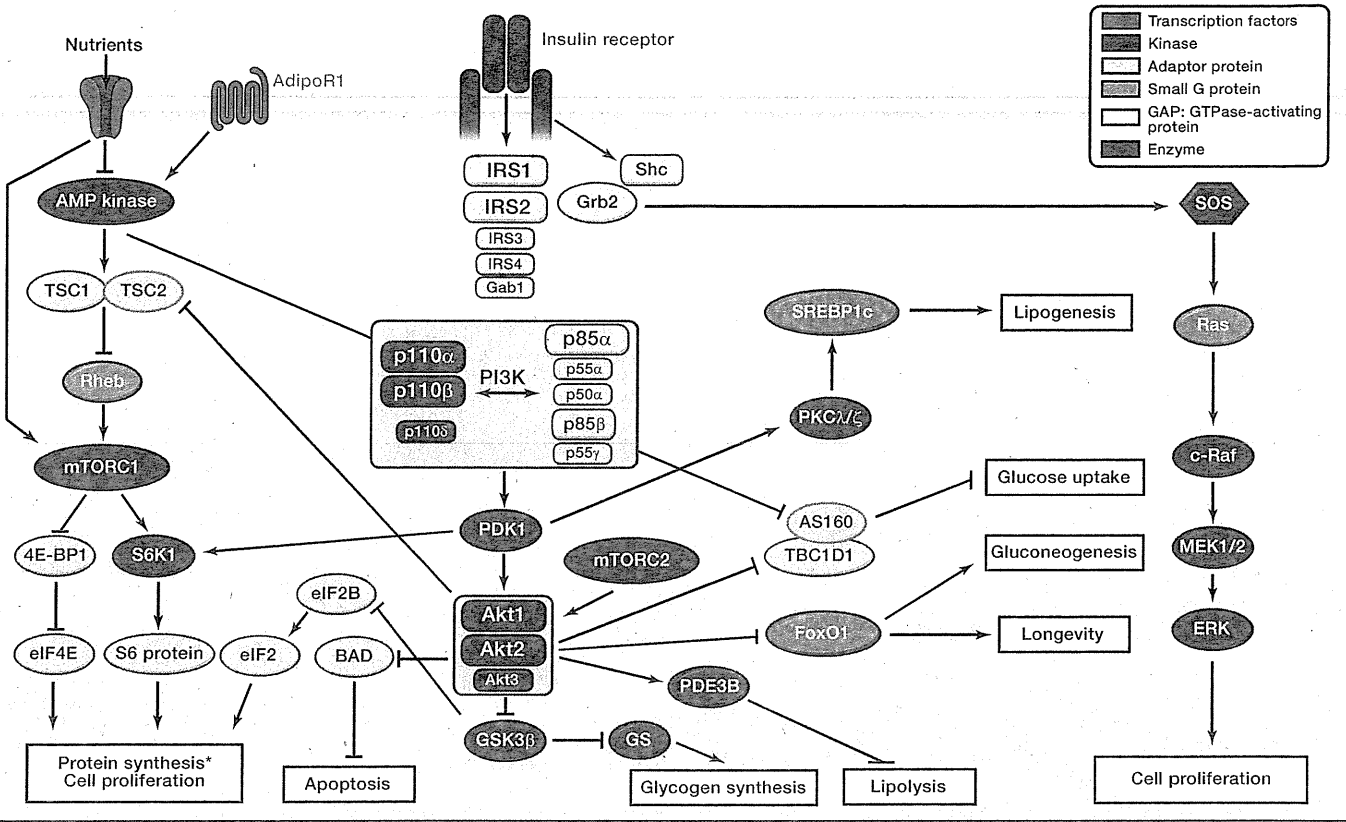

Negative regulatory mechanisms of insulin signaling

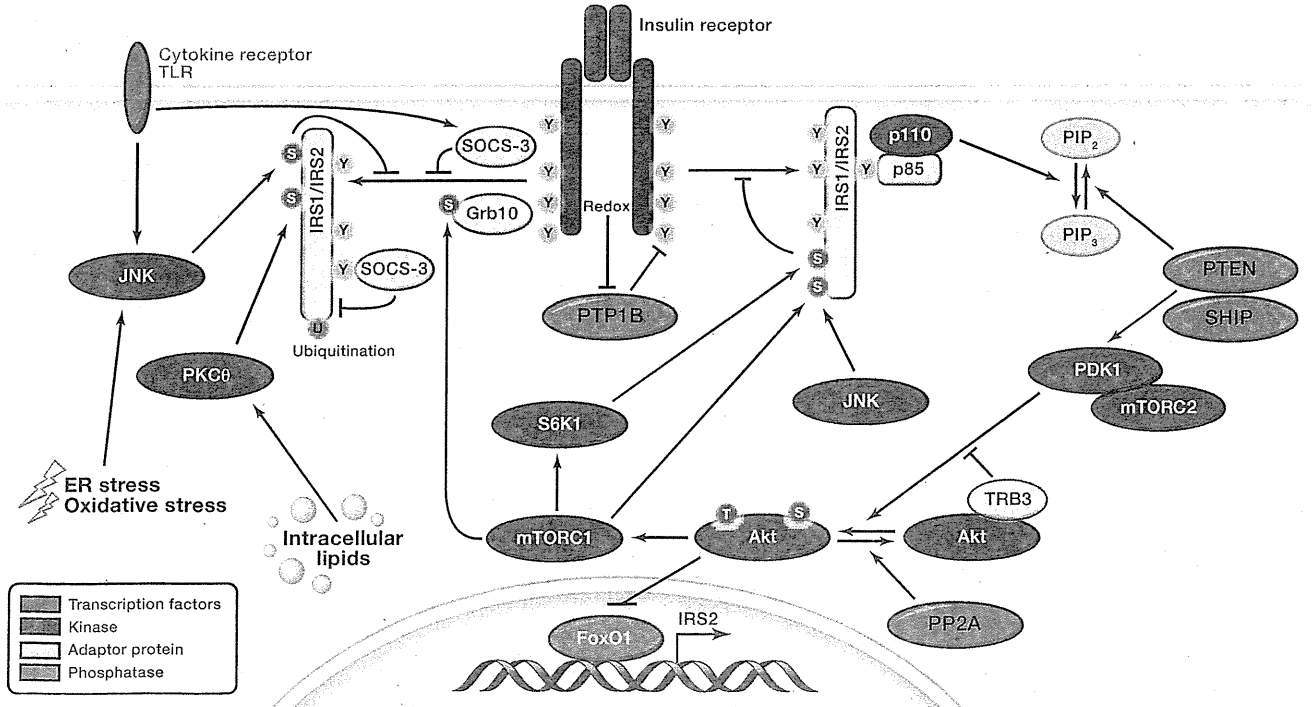

See online version for legend and references.

SnapShot: Insulin Signaling Pathways

Takashi Kadowaki, Kohjiro Ueki, Toshimasa Yamauchi, and Naoto Kubota
Department of Diabetes and Metabolic Diseases, Graduate School of Medicine, University of Tokyo, Bunkyo-ku, Tokyo 113-8655, Japan

Insulin Signaling through IRSs/PI3Ks/AKTs

Insulin binding to its receptor (IR) initiates a complex spectrum of biological effects in mammalian cells. Insulin binding activates the IR β subunit tyrosine kinase that phosphorylates IR substrate proteins (IRS proteins). The two major substrates, IRS-1 and IRS-2, are linked to the activation of the phosphatidylinositol 3-kinase (PI3K)-Akt pathway, which is responsible for most of the metabolic actions of insulin, and to the Ras-mitogen-activated protein kinase (MAPK) pathway, which cooperates with the PI3K pathway to control cell proliferation. IR can phosphorylate at least six known substrate proteins that are capable of interacting with five major forms of the PI3K regulatory subunit, which associate with three forms of the PI3K catalytic subunit. The subsequent generation of phosphatidylinositol-3,4,5-triphosphate (PIP3) leads to the activation of the three known isoforms of Akt via the PDK1 kinase. These combinatorial possibilities allow for the incredible diversification and fine-tuning of insulin signaling in normal physiology and disease states.

Metabolic Effects

Insulin signaling to Akt modulates a range of metabolic processes. In myocytes and adipocytes, phosphorylation of the Rab-GTPase-activating proteins AS160 (TBC1D4) and TBC1D1 by multiple kinases, including Akt, promotes glucose uptake. In hepatocytes, insulin-induced repression of genes involved in gluconeogenesis depends, at least in part, on Akt-mediated phosphorylation and inactivation of the forkhead transcription factor FoxO1. Moreover, insulin increases lipogenesis via kinase-dependent pathways involving PI3K, PDK1, PKCλ/ζ, and SREBP1c. It also increases glycogen synthesis via the GSK3β/glycogen synthase pathway and inhibits lipolysis via the Akt/PDE3B pathway.

Impact on Cell Proliferation and Death

In addition to metabolic effects, insulin has been reported to stimulate cell proliferation and to inhibit apoptosis. Tuberous sclerosis complex 1/2 is phosphorylated by several kinases, including Akt. Phosphorylation suppresses its GTPase-activating protein activity, leading to activation of the mTORC1 activator Rheb, a ras-like small GTPase, which ultimately results in increased cell proliferation through phosphorylation of S6K1 (p70 S6 kinase 1) and stimulation of translation. Insulin signaling also supports proliferation through activation of the Son-of-Sevenless (SOS)-initiated MAP kinase cascade. Insulin inhibits apoptosis via the Akt/BAD axis. Furthermore, insulin signaling in worms and flies has been shown to be involved in the negative regulation of life span via inhibition of FoxO1.

Interestingly, AMP kinase activation by adiponectin receptor signaling cooperates with the insulin signaling to increase glucose uptake via AS160 and/or TBC1D1, whereas this activation slows cell proliferation via inhibition of mTORC1.

Regulatory Control Mechanisms

Insulin signaling and the downstream pathways are subject to multilayered regulatory controls. These mechanisms include feedback loops and pathway responses to diverse stimuli.

Feedback Loops

Control of IR Activity. A nonreceptor-type phosphotyrosine phosphatase, PTP1B, dephosphorylates IR, limiting its activity. However, IR signaling produces H_2O_2 that inhibits PTP1B, leading to prolonged insulin signaling. An SH2-containing adaptor protein, Grb10, binds and inhibits IR kinase activity. Recently, mTORC1 has been shown to phosphorylate and enhance the inhibitory effect of Grb10 on IR.

At the IRS Level. Several serine/threonine kinases are known to phosphorylate and inhibit the recognition of IRS proteins by IR. S6K1 and mTORC1 phosphorylate serine residues of IRS-1, thereby inhibiting its tyrosine phosphorylation.

Effects on Downstream Pathways. PIP_3, a product of PI3K, is mainly degraded by two lipid phosphatases, PTEN (phosphatase and tensin homolog deleted from chromosome 10) and SHIP (src-homology 2-containing inositol 5′ phosphatase). At the Akt level, TRB3 (tribbles homolog 3) interacts with Akt, thereby inhibiting the recognition of Akt by PDK1 and mTORC2. Akt activity is also negatively regulated by PP2A (protein phosphatase 2A), which dephosphorylates two key phosphorylated resides, Thr308 and Ser473. Akt promotes nuclear excursion of FoxO1, leading to a rapid reduction of IRS-2 transcription, which is induced by FoxO1.

Induced Regulatory Mechanisms

Control of IR Activity. Proinflammatory cytokines acting through their receptors activate SOCS-3 (suppressor of cytokine signaling-3), which binds to IR and inhibits its ability to recognize IRS and initiate signaling.

At the IRS Level. JNK1 activated by various stimuli, such as cytokines, free fatty acids, ER stress, oxidative stress, and insulin, phosphorylates serine residues in the PTB domain of IRS-1, leading to a reduction of tyrosine phosphorylation. PKCθ activated by intracellular lipid accumulation phosphorylates the same residues of IRS-1. Beyond its interaction with the receptor, SOCS-3 also binds to IRS proteins and functions as a ubiquitin ligase, inducing their degradation and reducing their signaling.

REFERENCES

Cohen, P. (2006). The twentieth century struggle to decipher insulin signalling. Nat. Rev. Mol. Cell Biol. *7*, 867–873.

Cross, D.A., Alessi, D.R., Cohen, P., Andjelkovich, M., and Hemmings, B.A. (1995). Inhibition of glycogen synthase kinase-3 by insulin mediated by protein kinase B. Nature *378*, 785–789.

Kasuga, M., Karlsson, F.A., and Kahn, C.R. (1982). Insulin stimulates the phosphorylation of the 95,000-dalton subunit of its own receptor. Science *215*, 185–187.

Kadowaki, T. (2000). Insights into insulin resistance and type 2 diabetes from knockout mouse models. J. Clin. Invest. *106*, 459–465.

Kyriakis, J.M., App, H., Zhang, X.F., Banerjee, P., Brautigan, D.L., Rapp, U.R., and Avruch, J. (1992). Raf-1 activates MAP kinase-kinase. Nature *358*, 417–421.

Lin, H.V., and Accili, D. (2011). Hormonal regulation of hepatic glucose production in health and disease. Cell Metab. *14*, 9–19.

Ruderman, N.B., Kapeller, R., White, M.F., and Cantley, L.C. (1990). Activation of phosphatidylinositol 3-kinase by insulin. Proc. Natl. Acad. Sci. USA *87*, 1411–1415.

Taniguchi, C.M., Emanuelli, B., and Kahn, C.R. (2006). Critical nodes in signalling pathways: insights into insulin action. Nat. Rev. Mol. Cell Biol. *7*, 85–96.

Tonks, N.K. (2005). Redox redux: revisiting PTPs and the control of cell signaling. Cell *121*, 667–670.

Yamauchi, T., Kamon, J., Ito, Y., Tsuchida, A., Yokomizo, T., Kita, S., Sugiyama, T., Miyagishi, M., Hara, K., Tsunoda, M., et al. (2003). Cloning of adiponectin receptors that mediate antidiabetic metabolic effects. Nature *423*, 762–769.

Impact of the Dipeptidyl Peptidase-4 Inhibitor Vildagliptin on Glucose Tolerance and β-Cell Function and Mass in Insulin Receptor Substrate-2-Knockout Mice Fed a High-Fat Diet

Koichiro Sato, Akinobu Nakamura, Jun Shirakawa, Tomonori Muraoka, Yu Togashi, Kazuaki Shinoda, Kazuki Orime, Naoto Kubota, Takashi Kadowaki, and Yasuo Terauchi

Department of Endocrinology and Metabolism (K.S., A.N., J.S., T.M., Y.To., K.S., K.O., Y.Te.), *Graduate* School of Medicine, Yokohama City University, Japan; and Department of Diabetes and Metabolic Diseases (N.K., T.K.), Graduate School of Medicine, University of Tokyo, Tokyo 113-8655, Japan

Type 2 diabetes is characterized by diminished pancreatic β-cell mass and function. Glucagon-like peptide-1 has been reported to increase islet cell proliferation and reduce apoptosis of β-cells in rodents. In this study, we explored the effect of chronic administration of the dipeptidyl peptidase-4 inhibitor vildagliptin on glucose tolerance, β-cell function, and β-cell mass in *Irs2*-knockout ($Irs2^{-/-}$) mice. Wild-type and $Irs2^{-/-}$ mice were fed a high-fat diet for 20 wk, with or without vildagliptin. In both genotypes of mice, vildagliptin significantly decreased the area under the curve (0–120 min) of blood glucose and increased the insulin response to glucose during the oral glucose tolerance test. In the oral glucose tolerance test performed 1 d after discontinuation of vildagliptin administration, the area under the curve (0–120 min) of blood glucose was still significantly decreased and the insulin response to glucose was significantly increased in the $Irs2^{-/-}$ mice treated with vildagliptin as compared with the values in the mice not treated with vildagliptin. Histochemical analysis of the pancreatic islets revealed significant increase of the β-cell mass and decrease in the proportion of terminal deoxynucleotidyl transferase dUTP nick end labeling-positive β-cells but no significant increase of the bromodeoxyuridine incorporation in $Irs2^{-/-}$ mice treated with vildagliptin. Our results suggest that vildagliptin improved glucose tolerance and increased the β-cell mass by reducing β-cell apoptosis in the $Irs2^{-/-}$ mice, and that the reduction of β-cell apoptosis by vildagliptin was independent of the *Irs2* expression in the cells. **(*Endocrinology* 153: 1093–1102, 2012)**

Type 2 diabetes mellitus is a chronic metabolic disease caused by peripheral insulin resistance and impaired insulin secretion by the pancreatic β-cells (1, 2). In subjects predisposed to diabetes, blood glucose levels are maintained within the normal range by compensatory increase of the β-cell mass and/or function in response to insulin resistance. Diabetes develops only in subjects that are unable to sustain the compensatory β-cell response (3). Indeed, most individuals with type 2 diabetes, whether obese or lean, show a net decrease of the β-cell mass (4). However, the mechanism of increase of the β-cell mass in response to insulin resistance is not yet fully understood, and precise clarification of this mechanism is required for developing effective strategies for the treatment of diabetes mellitus.

Insulin receptor substrate-2 (Irs2) is one of the major substrates of insulin receptor tyrosine kinase and IGF receptor kinase (5). *Irs2*-knockout ($Irs2^{-/-}$) mice develop

ISSN Print 0013-7227 ISSN Online 1945-7170
Printed in U.S.A.

doi: 10.1210/en.2011-1712 Received September 1, 2011. Accepted December 28, 2011.
First Published Online February 7, 2012

Abbreviations: AUC, Area under the curve; BrdU, bromodeoxyuridine; CREB, cAMP response element-binding protein; DPP-4, dipeptidyl peptidase-4; GIP, glucose-dependent insulinotropic polypeptide; GLP, glucagon-like peptide; GSIS, glucose-stimulated insulin secretion; HF, high-fat; Irs2, insulin receptor substrate-2; OGTT, oral glucose tolerance test; TUNEL, terminal deoxynucleotidyl transferase dUTP nick end labeling; WAT, white adipose tissue.

type 2 diabetes in association with hepatic insulin resistance and lack of compensatory β-cell hyperplasia (6). We previously demonstrated that wild-type mice administered a high-fat diet showed marked β-cell hyperplasia to compensate for the insulin resistance, whereas mice with haploinsufficiency of Irs2 ($Irs2^{+/-}$) and homozygous deletion of Irs2 ($Irs2^{-/-}$) showed insufficient β-cell hyperplasia (7). In high-fat (HF) diet-fed mice with haploinsufficiency of β-cell- and brain-specific glucokinase ($Gck^{+/-}$), which show decreased β-cell proliferation and insufficient β-cell hyperplasia in response to insulin resistance, overexpression of Irs2 in the β-cells partially prevented diabetes by inducing β-cell proliferation (7). These results suggest that Irs2 could play a pivotal role in regulating β-cell proliferation in response to HF diet-induced insulin resistance. Moreover, Irs2 is known to play an important role in protecting against apoptosis (8, 9). Increased numbers of apoptotic cells were present in the islets of $Irs2^{-/-}$ mice as compared with those in wild-type mice (8), and expression of Irs2 protected β-cells from transcription factor 3-induced apoptosis (9).

Incretins are peptide hormones secreted after meal ingestion that potentiate glucose-stimulated insulin secretion. The two predominant incretins are glucagon-like peptide (GLP)-1 and glucose-dependent insulinotropic polypeptide (GIP) (10). Human recombinant GLP-1 has been shown not only to enhance glucose-stimulated insulin secretion, but also to increase islet cell proliferation and β-cell mass and decrease cellular apoptosis in rodents (11). In addition, its effect of chronic administration upon β-cell growth and survival are thought to be mediated by Irs2 (9, 12). However, both GLP-1 and GIP are rapidly degraded and inactivated *in vivo*, primarily by the enzyme dipeptidyl peptidase-4 (DPP-4) (13). Therefore, DPP-4 inhibitors to prolong the effects of endogenous incretins began to be developed as a novel strategy (14). Vildagliptin is a DPP-4 inhibitor that was shown to improve glucose tolerance in both rodents and humans with type 2 diabetes and has gained approval around the world as a new class of drugs for the treatment of type 2 diabetes mellitus (15–18). However, little is known about whether vildagliptin can also increase the pancreatic β-cell mass and whether Irs2 might be involved in the effect of chronic administration of vildagliptin on the β-cell mass (16, 19, 20). We therefore examined the metabolic consequences of chronic administration of the DPP-4 inhibitor vildagliptin for 20 wk in wild-type and $Irs2^{-/-}$ mice fed a HF diet.

Materials and Methods

Animals

$Irs2^{-/-}$ mice generated by Kubota *et al.* (6) were backcrossed with C57BL/6J mice for more than 10 generations. Wild-type and $Irs2^{-/-}$ mice were prepared by intercrossing of $Irs2^{+/-}$ mice. Each of the genotypes of mice derived from the same genetic background were fed standard chow until 8 wk of age and then given free access to a HF diet for 20 wk. Half of the animals of each genotype were given vildagliptin mixed in their drinking water (0.3 mg/ml), whereas the remaining half were given tap water not containing vildagliptin. All experiments in this study were performed using male littermates. The animals were maintained by standard animal care procedures based on the institutional guideline. The animal housing rooms were maintained at a constant room temperature (25 C) and under a 12-h light (0800 h), 12-h dark (2000 h) cycle.

Diet protocol

The compositions of the standard chow and HF diet (CLEA Rodent Diet CE-2 and High Fat Diet 32, respectively; Clea Japan, Inc., Tokyo, Japan) have been described previously (7, 21). Half of the animals in each genotype were given the DPP-4 inhibitor vildagliptin (kindly gifted by Novartis Pharmaceuticals Corporation, East Hanover, NJ) mixed in drinking water (0.3 mg/ml, ~3 μmol vildagliptin/d·mouse, a dosing regimen previously demonstrated to provide >80–90% inactivation of the plasma DPP-4 activity throughout the day) (22).

Measurement of the biochemical parameters

Blood glucose was measured by a portable glucose meter using Glutest Neo (Sanwa Chemical Co., Nagoya, Japan). Insulin levels were determined with an insulin ELISA kit (Morinaga Institute of Biological Science, Inc., Yokohama, Japan). Plasma levels of free fatty acid, total cholesterol, and triglycerides were assayed by enzymatic methods (Wako Pure Chemical Industries Ltd., Osaka, Japan).

Oral glucose tolerance test (OGTT)

Mice denied access to food for more than 18 h before the study were loaded orally with glucose at 1.5 mg/g body weight. Blood samples were collected from the tail before and 15, 30, 60, and 120 min after the glucose loading. Blood glucose levels were determined using Glutest Neo (Sanwa). Whole blood was collected and centrifuged in heparinized tubes, and the plasma was stored at −20 C. Plasma insulin levels were determined using an insulin ELISA kit (Morinaga Institute of Biological Science) with mouse insulin as a standard.

Insulin tolerance test

The insulin tolerance test was performed without denying animal access to food. Insulin (1.5 mU/g body weight) was injected ip, and blood samples were collected from the tail before and 30, 60, 90, and 120 min after the injection.

Glucose-stimulated insulin secretion (GSIS) by the islets

Islets were isolated with collagenase XI (Sigma-Aldrich Co., St. Louis, MO) 2 d after discontinuation of vildagliptin administration. Immediately or after culture for 12 h in RPMI 1640 medium containing 11 mM glucose supplemented with 10% fetal calf serum, 100 U/ml penicillin, and 100 μg/ml streptomycin

(Sigma), 10 islets were incubated at 37 C for 1.5 h in Krebs-Ringer bicarbonate buffer containing 2.8, 8.3, or 22.2 mM glucose. The isolated islets were extracted in acid ethanol, and their insulin content was measured as described previously, with slight modifications (6). The insulin concentration of the assay buffer was measured using an insulin ELISA kit (Morinaga Institute of Biological Science).

Immunohistochemical analysis for estimation of the β-cell mass

Isolated pancreata were immersion-fixed overnight in 10% formalin at 4 C. The tissue specimens were then routinely processed for paraffin embedding, and 4-μm sections mounted on glass slides were immunostained with rabbit antihuman insulin (diluted 1:1000) antibody (Santa Cruz Biotechnology Inc., Santa Cruz, CA). The area of the β-cells relative to the area of the whole pancreatic tissue was calculated with the Win ROOF software (Mitani Corp., Tokyo, Japan), as described elsewhere (7, 23). The sections were immunostained with antibodies to glucagon (Abcam, Cambridge, UK) and insulin (Santa Cruz Biotechnology), and Alexa Fluor 488- and 555-conjugated secondary antibodies (Invitrogen, Carlsbad, CA) were used for the fluorescence microscopy. The images were acquired using an Olympus FV1000-D confocal laser scanning microscope. Approximately 100 islets per mouse were counted in each group.

Analysis of bromodeoxyuridine (BrdU) incorporation

BrdU incorporation was analyzed as described previously (7). In brief, BrdU (100 mg/kg in PBS; Nacalai Tesque, Inc., Kyoto, Japan) was injected ip, and the pancreas was removed 6 h later. The sections were double immunostained with anti-BrdU antibody (diluted 1:10) (BD Biosciences, San Diego, CA) and anti-insulin antibody (diluted 1:1000). BrdU-positive β-cells were quantitatively assessed as a percentage of the total number of β-cells by counting 50–150 islets per mouse.

Detection of apoptotic cells

Apoptotic cells were detected in deparaffinized pancreatic tissue sections by the terminal deoxynucleotidyl transferase dUTP nick end labeling (TUNEL) method using an ApopTag (Chemicon International Inc., Temecula, CA), according to the manufacturer's recommendations. Sections were also immunostained for insulin and counterstained with 4′,6-diamidino-2-phenylindole. TUNEL-positive β-cells were counted as insulin-stained cells and divided by the total number of β-cells.

Real-time PCR

For preparation for the mRNA, islets were isolated with collagenase XI (Sigma-Aldrich) (24). cDNA was prepared using the TaqMan reverse transcriptase kit (Applied Biosystems, Carlsbad, CA) and subjected to quantitative PCR by performing TaqMan gene expression assays using the Universal Master Mix (7500 real-time PCR system; Applied Biosystems). All probes used in the TaqMan gene expression assays were purchased from Applied Biosystems. Each quantitative reaction was performed in duplicate. The data were normalized to the values for β-actin.

Western blot analysis

For immunoblotting, isolated islets (120 islets) were lysed in ice-cold radioimmune precipitation assay buffer (Cell Signaling Technology, Inc., Danvers, MA) with Complete protease inhibitor mixture (Roche Diagnostics, Tokyo, Japan). After centrifugation, the extracts were subjected to immunoblotting with antibodies to Bcl-2 (Trevigen, Inc., Gaithersburg, MD), Bax (Santa Cruz), cleaved caspase-3 and caspase-3 (Cell Signaling Technology), and glyceraldehyde-3-phosphate dehydrogenase (Abcam). Densitometry was performed using NIH ImageJ software.

Statistics

Results are expressed as means ± SEM (n). Statistical analysis was performed using Microsoft Excel Statistics 2003 for Windows (SSRI Co., Ltd., Tokyo, Japan) and SPSS version 11 (SPSS Inc., Chicago, IL). Differences between two groups were analyzed for statistical significance by Student's t test or ANOVA. $P < 0.05$ was considered as indicative of statistical significance.

Results

Vildagliptin decreased fasting blood glucose in the *Irs2*$^{-/-}$ mice

To investigate the effect of vildagliptin on the body weight and blood glucose levels, the mice were not treated or treated with vildagliptin mixed in their drinking water. After 20 wk of treatment, there were no differences in the body weight as compared with that of the control mice in any of the genotypes of the mice (Fig. 1A). No significant differences in the epididymal white adipose tissue (WAT), retroperitoneal WAT, mesenteric WAT, sc WAT, or liver weight were observed between the control mice and the treated mice of any genotype, except for the epididymal WAT in the *Irs2*$^{-/-}$ mice and retroperitoneal WAT in the wild-type mice (Table 1). Vildagliptin also had no effect on the food intake in any of the genotypes of mice (Fig. 1B). The fasting blood glucose tended to be higher in the *Irs2*$^{+/-}$ mice and was significantly higher in *Irs2*$^{-/-}$ mice as compared than that in the wild-type mice. Wild-type mice treated with vildagliptin for 20 wk showed fasting blood glucose levels similar to wild-type mice not treated with vildagliptin; on the other hand, the fasting blood glucose levels in the *Irs2*$^{+/-}$ mice treated with vildagliptin tended to be lower than those in the *Irs2*$^{+/-}$ mice not treated with vildagliptin and the levels in the *Irs2*$^{-/-}$ mice treated with vildagliptin were significantly lower than the levels in the *Irs2*$^{-/-}$ mice not treated with vildagliptin (Fig. 1C). No significant differences in the plasma lipid parameters or triglyceride contents in the liver were observed between the untreated and

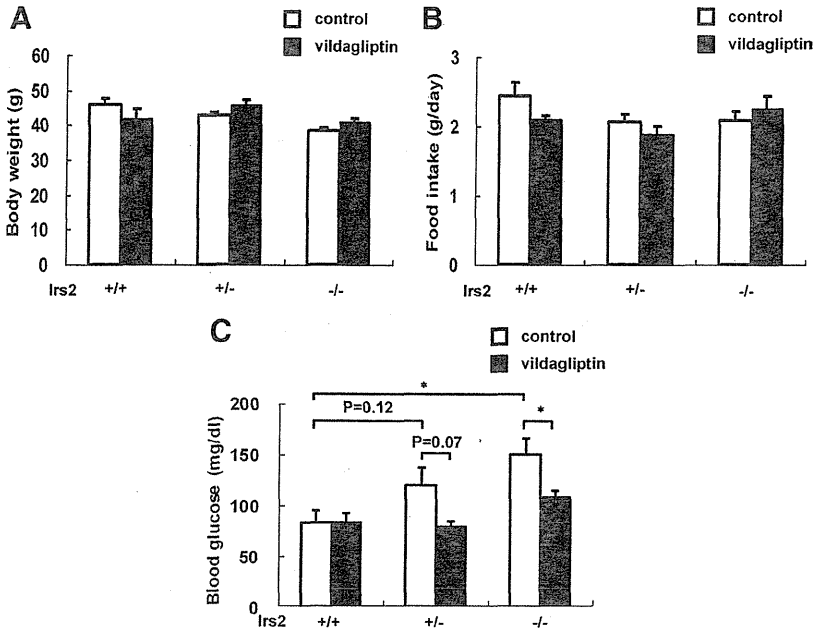

FIG. 1. Vildagliptin had no significant effect on the body weight gain or food intake but reduced the fasting blood glucose in *Irs2*$^{-/-}$ mice. A–C, Body weight (A), food intake (B), and fasting blood glucose (C) in the wild-type, *Irs2*$^{+/-}$, and *Irs2*$^{-/-}$ mice after 20 wk on a HF diet (n = 5- 7). *, $P < 0.05$. The results are presented as the mean ± SE.

treated mice of any genotype, except for the low-density lipoprotein cholesterol in the *Irs2*$^{+/-}$ mice and free fatty acid in the *Irs2*$^{-/-}$ mice (Table 1).

Vildagliptin improved glucose tolerance

Vildagliptin treatment for 20 wk significantly reduced the glycemic excursions after oral glucose loading in all the genotypes of mice, which was correlated with the increase in the plasma levels of insulin 15 min after the oral glucose load (Fig. 2, A–D). To investigate whether long-term treatment with vildagliptin *per se* might have contributed to the improvement of the glucose tolerance, we also performed OGTT 1 d after discontinuation of vildagliptin administration. The area under the curve $(AUC)_{0-120min}$ of blood glucose was still significantly decreased, and the insulin response to glucose 15 min after the oral glucose load was significantly increased in both *Irs2*$^{+/-}$ and *Irs2*$^{-/-}$ mice treated with vildagliptin as compared with those in the corresponding mouse genotypes not treated with vildagliptin. Meanwhile, the $AUC_{0-120min}$ of blood glucose was not significantly decreased, and the insulin response to glucose 15 min after the oral glucose load was not significantly increased in the wild-type mice treated with vildagliptin as compared with those without vildagliptin in the OGTT performed 1 d after discontinuation of vildagliptin administration.

Then, to assess the effect of vildagliptin on the insulin sensitivity, we performed the insulin tolerance test. Among the wild-type mice, the blood glucose levels in the vildagliptin-treated group at 60, 90, and 120 min after the injection were significantly lower than those in the untreated control group (Fig. 2E). Among the *Irs2*$^{+/-}$ and *Irs2*$^{-/-}$ mice, the blood glucose levels before the injection in the treated groups were already lower than those in the untreated control groups, and there were no differences in the blood glucose levels at any time point after the insulin injection (Fig. 2, F and G).

TABLE 1. WAT and liver weight relative to the body weight, plasma lipid parameters, and triglyceride content of the liver in wild-type, *Irs2*$^{+/-}$, and *Irs2*$^{-/-}$ mice

	Wild-type		*Irs2*$^{+/-}$		*Irs2*$^{-/-}$	
	Control	Vildagliptin	Control	Vildagliptin	Control	Vildagliptin
WAT						
Epididymal	30.4 ± 2.5	30.1 ± 2.4	31.7 ± 2.8	27.8 ± 2.6	34.4 ± 1.3	27.6 ± 1.3[a]
Retroperitoneal	15.0 ± 1.0	9.8 ± 0.7[a]	10.3 ± 0.4	9.5 ± 0.9	8.7 ± 0.9	7.5 ± 1.1
Mesenteric	26.7 ± 1.2	20.3 ± 3.4	18.3 ± 0.6	19.2 ± 0.3	18.1 ± 1.5	15.8 ± 1.0
Subcutaneous	66.9 ± 3.4	54.2 ± 5.5	49.6 ± 2.9	57.3 ± 3.0	41.5 ± 2.8	44.9 ± 3.3
Total	139.7 ± 4.6	114.3 ± 10.4	110.0 ± 3.0	113.8 ± 5.9	102.7 ± 4.0	95.8 ± 5.8
Liver	67.1 ± 7.5	50.3 ± 6.6	54.5 ± 3.8	61.8 ± 4.1	57.9 ± 3.0	58.0 ± 2.8
Total cholesterol (mg/dl)	215.8 ± 22.1	168.2 ± 25.9	144.0 ± 8.6	128.3 ± 11.6	164.0 ± 13.2	141.4 ± 15.4
Triglyceride (mg/dl)	58.4 ± 7.2	46.5 ± 4.9	35.4 ± 3.3	29.7 ± 4.2	32.3 ± 5.3	21.6 ± 3.8
LDL cholesterol (mg/dl)	125.2 ± 17.0	95.5 ± 17.0	88.3 ± 4.4	58.6 ± 9.8[a]	81.3 ± 8.5	64.9 ± 8.4
Free fatty acid (mEq/liter)	2.19 ± 0.27	1.69 ± 0.21	1.62 ± 0.11	1.39 ± 0.15	1.61 ± 0.08	1.27 ± 0.09[a]
TG content in the liver (mg/g tissue)	190.9 ± 13.3	136.3 ± 30.3	120.8 ± 24.7	143.4 ± 6.3	114.3 ± 11.5	124.2 ± 5.0

Each WAT and liver are represented as (1000 × respective weight/body weight). Data represent means ± SE; n = 5–7. LDL, Low-density lipoprotein; TG, triglyceride.

[a] $P < 0.05$ relative to control.

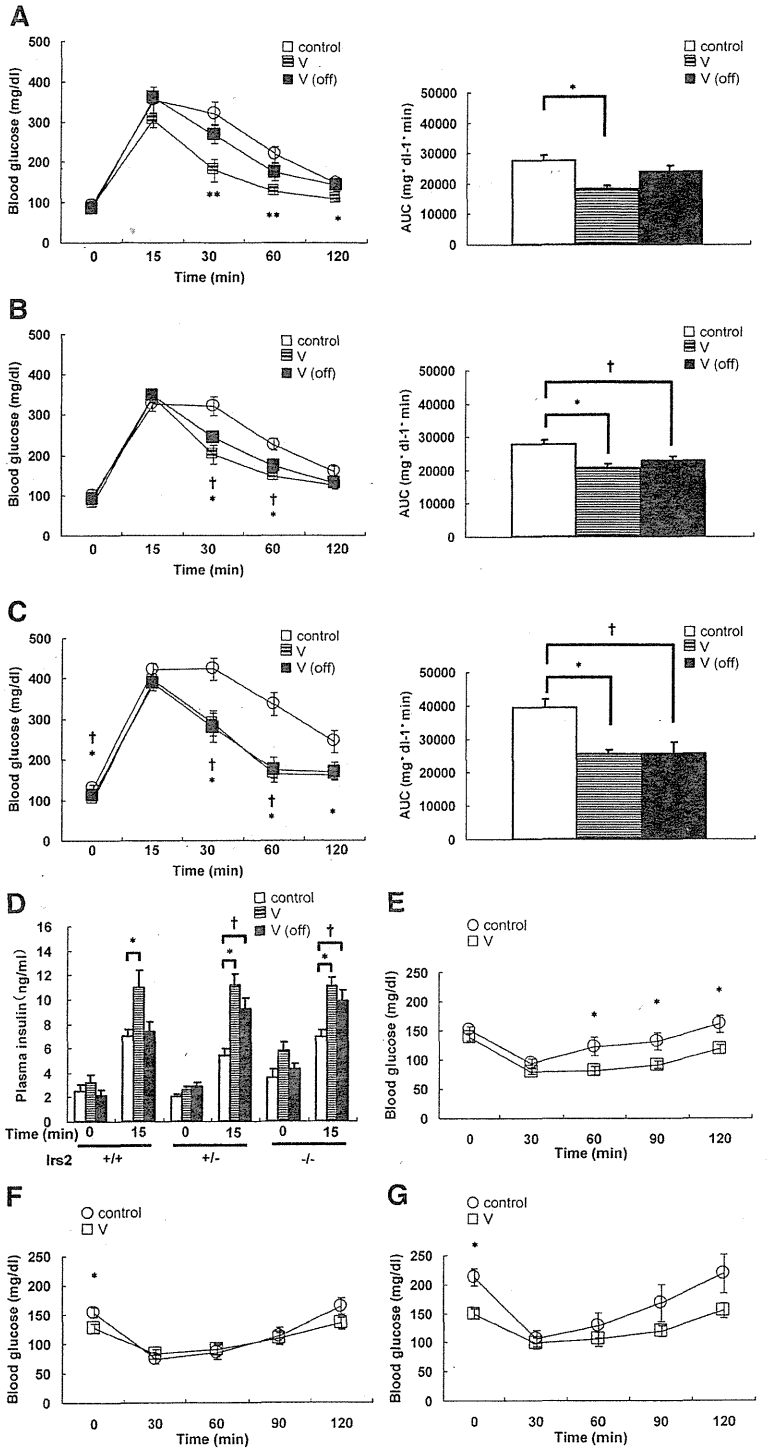

FIG. 2. Twenty weeks of vildagliptin treatment improved the glucose tolerance as determined by an OGTT. A–C, OGTT was performed in wild-type (A), $Irs2^{+/-}$ (B), and $Irs2^{-/-}$ (C) mice after 20 wk of vildagliptin (V) treatment (n = 6- 10). AUC was calculated for the glucose excursions during the OGTT from 0–120 min. D, Plasma insulin levels in the wild-type, $Irs2^{+/-}$, and $Irs2^{-/-}$ mice after 20 wk of vildagliptin treatment (n = 6- 10). V (off), Mouse group in which the OGTT was performed 1 d after discontinuation of administration of vildagliptin. E–G, Insulin tolerance test results in the wild-type (E), $Irs2^{+/-}$ (F), and $Irs2^{-/-}$ (G) mice after 20 wk of vildagliptin treatment (n = 10). *, Statistical significance ($P < 0.05$) for the V group *vs.* control; **, statistical significance ($P < 0.01$) for the V group *vs.* control; †, statistical significance ($P < 0.05$) for the V (off) group *vs.* control. The results are presented as the mean ± SE.

Ex vivo evaluation of the islet insulin content and function

The effects of chronic DPP-4 inhibitor administration in the function of the pancreatic islets were evaluated using islets isolated from animals treated for 20 wk with vildagliptin. To evaluate the effects of chronic administration of vildagliptin, rather than its direct effects, on the β-cells, we isolated islets 2 d after discontinuation of vildagliptin administration. In the absence of vildagliptin treatment, the islet insulin content of the $Irs2^{-/-}$ mice was significantly decreased as compared with that of the wild-type mice, and that of the $Irs2^{+/-}$ mice was decreased by 16% as compared with the value for the wild-type mice. Although the islet insulin content was indistinguishable between the wild-type mice treated and not treated with vildagliptin, the islet insulin content of the $Irs2^{-/-}$ mice treated with vildagliptin was significantly increased as compared with that of the untreated control mice, and there was also a trend toward increase in the $Irs2^{+/-}$ mice treated with vildagliptin (Fig. 3A).

Then, we assessed the GSIS of each genotype of mice after 20 wk of treatment. There were no differences in the GSIS between the untreated control and treated wild-type or $Irs2^{+/-}$ mice. The insulin secretory response to 8.3 and 22.2 mM glucose in the $Irs2^{-/-}$ mice treated with vildagliptin was increased by 34 and 35%, respectively, as compared with that in the untreated control mice, although the difference was not statistically significant (Fig. 3B). When we calculated the insulin secretory responses normalized by the islet insulin content, no improvement of the GSIS was observed in any of the genotypes of mice (Fig. 3C).

Increased β-cell mass in the islets of the $Irs2^{-/-}$ mice

In the absence of vildagliptin treatment, the β-cell mass of the $Irs2^{-/-}$ mice was significantly decreased as

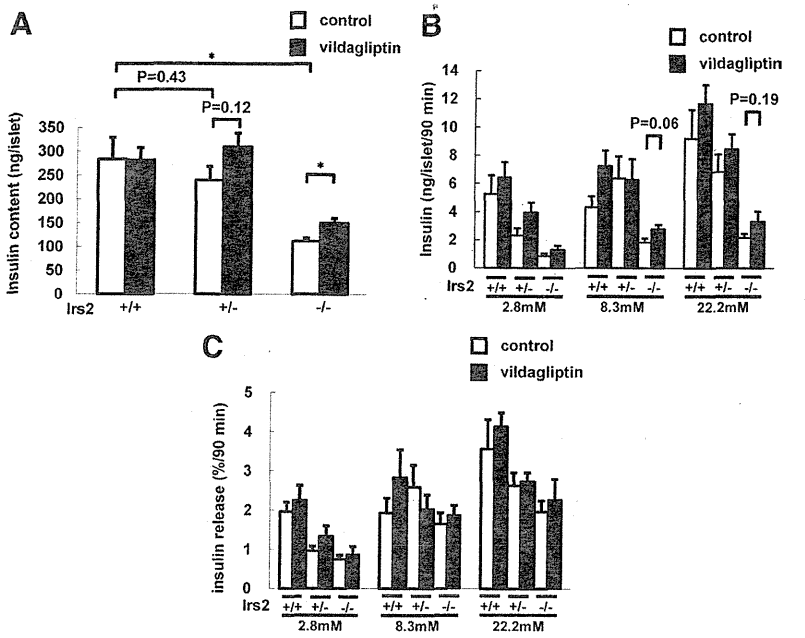

FIG. 3. *Ex vivo* analyses of pancreatic islets. Islets were isolated from wild-type, $Irs2^{+/-}$, and $Irs2^{-/-}$ mice after 20 wk of vildagliptin treatment. A, The insulin content in the islets was determined after acid ethanol extraction; B and C, insulin secretory responses to 2.8, 8.3, and 22.2 mM glucose (B) and the insulin secretory ratio adjusted by the insulin content (C) were determined by 90-min static incubations in Krebs-Ringer bicarbonate buffer medium (n = 5). *, $P < 0.05$. The results are presented as the mean ± SE.

compared with that of the wild-type mice, and that of the $Irs2^{+/-}$ mice was decreased by 19% as compared with the value for the wild-type mice. To assess the effect of chronic administration of vildagliptin on the pancreatic islets, we measured the β-cell mass of each genotype of mice after 20 wk of treatment. Although vildagliptin exerted no effect on the β-cell mass in the wild-type mice, the β-cell mass of the $Irs2^{-/-}$ mice treated with vildagliptin was significantly increased as compared with that of the mice not treated with vildagliptin, and there was also a trend toward increase in the mass in the $Irs2^{+/-}$ mice (Fig. 4A). Then, we measured the α-cell mass of each genotype of mice after 20 wk of treatment. In the absence of vildagliptin treatment, each genotype of mice showed similar values of the α-cell mass, and there were no differences in the α-cell mass between the untreated control mice and treated mice, irrespective of the genotype (Fig. 4B). When we calculated the ratio of the β-cell area to the total area of α- and β-cells in the wild-type mice, the treated group showed a ratio similar to that in the untreated control group. In the $Irs2^{-/-}$ mice, the ratio in the treated group was significantly increased as compared with that in the untreated control group, and there was also a trend toward increase in the $Irs2^{+/-}$ mice (Fig. 4C).

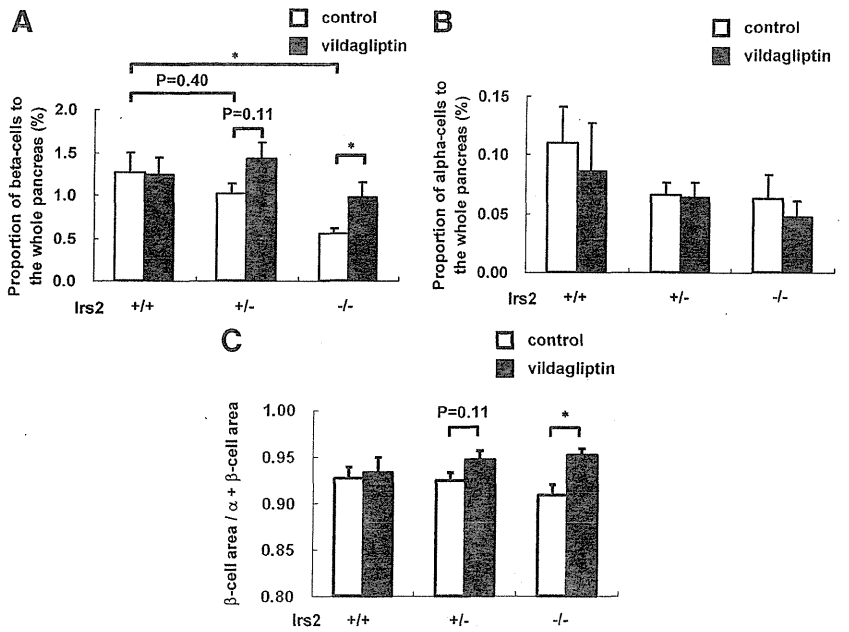

FIG. 4. Twenty weeks of vildagliptin treatment increased the β-cell mass in $Irs2^{-/-}$ mice. A, Insulin-positive β-cell area relative to the whole pancreatic area (n = 5- 8); B, glucagon-positive α-cell area relative to the whole pancreatic area (n = 5); C, ratios of the insulin-positive β-cell area to the sum of the glucagon-positive α-cell area plus the insulin-positive β-cell area (n = 5- 8). *, $P < 0.05$. The results are presented as the mean ± SE.

Vildagliptin protected the β-cells of the $Irs2^{-/-}$ mice from apoptosis

To determine the mechanism of increase of the β-cell mass by vildagliptin treatment in the $Irs2^{-/-}$ mice, we first assessed the proliferative activity of the β-cells. In the absence of vildagliptin treatment, $Irs2^{-/-}$ mice showed a significant decrease in the ratio of BrdU-positive β-cells as compared with that in the wild-type mice, and vildagliptin had no effect on the ratio of the BrdU-positive β-cells in either genotype of mice (Fig. 5A). We next assessed the apoptotic activity of the β-cells. In the absence of vildagliptin treatment, $Irs2^{-/-}$ mice showed a significant increase in the percentage of TUNEL-positive β-cells as compared with that in the wild-type mice (Fig. 5B). Although there was no difference in the percentage of TUNEL-positive β-cells between the untreated control and treated wild-

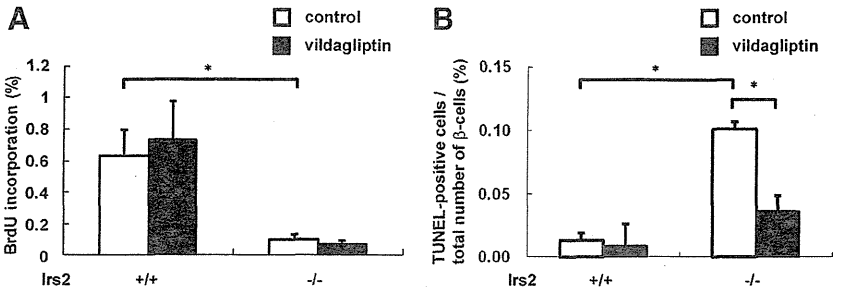

FIG. 5. Twenty weeks of vildagliptin treatment failed to increase the number of BrdU-positive β-cells, but reduced the number of TUNEL-positive β-cells in the *Irs2*$^{-/-}$ mice. A, Percentage of BrdU-positive β-cells relative to the total number of β-cells (n = 5); B, percentage of TUNEL-positive β-cells relative to the total number of β-cells (n = 5). *, $P < 0.05$. The results are presented as the mean ± SE.

type mice, the percentage of TUNEL-positive β-cells was significantly decreased in the *Irs2*$^{-/-}$ mice treated with vildagliptin as compared with that in the same genotype of mice not treated with vildagliptin.

Vildagliptin increased the mRNA expression level of *bcl-2* in the *Irs2*$^{-/-}$ mice

To determine how vildagliptin protected against β-cell apoptosis in the *Irs2*$^{-/-}$ mice, we assessed the mRNA expression levels of markers of apoptosis or endoplasmic reticulum stress in the wild-type mice and *Irs2*$^{-/-}$ mice. Vildagliptin had no effect on the expression levels of *bax* or *chop* in either genotype of mice (Fig. 6A). Although there was no difference in the *bcl-2* mRNA level between the control untreated group and the treated among the wild-type mice, the *bcl-2* mRNA expression levels were significantly increased in the *Irs2*$^{-/-}$ mice treated with vildagliptin. The protein expression levels in islets after 20 wk of treatment were also evaluated. No significant differences in the expression levels of Bcl-2, Bax. and cleaved caspase-3 were observed between the control mice and the treated mice of both genotypes (Fig. 6B).

Discussion

Ever since the discovery of DPP-4 inhibitors, numerous studies have demonstrated the antidiabetic efficacy of these agents in rodents (25, 26). The effect of chronic administration of vildagliptin on glucose metabolism, however, had not been clarified. We, as well as others, had

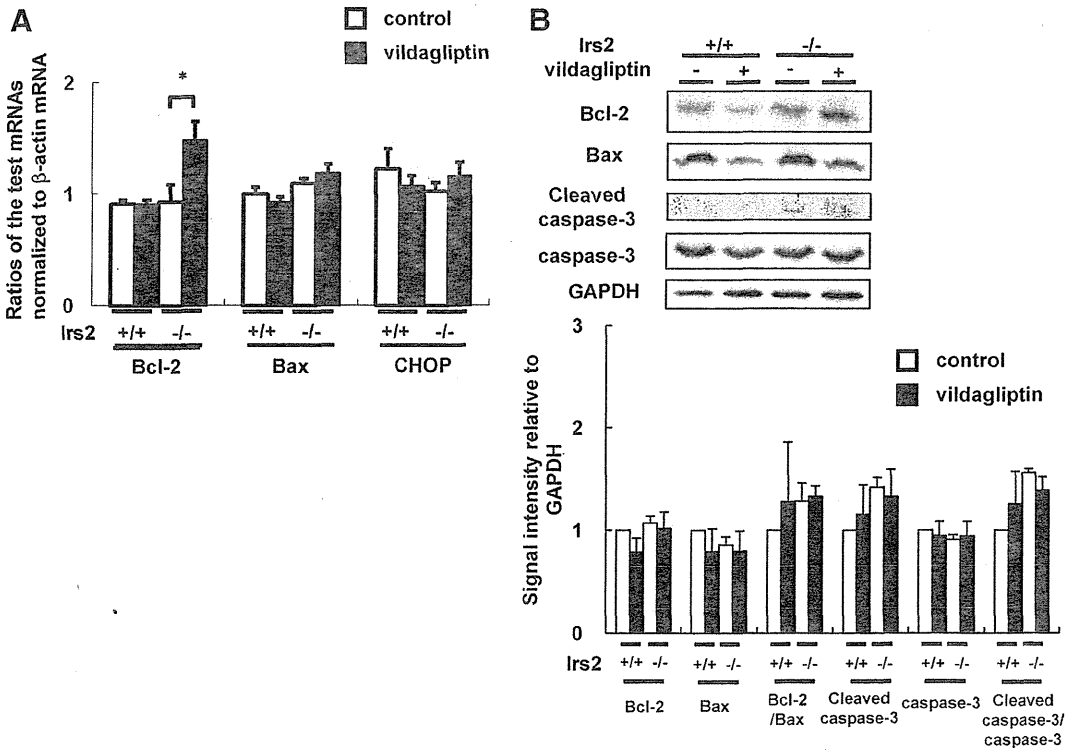

FIG. 6. Twenty weeks of vildagliptin treatment increased the mRNA expression level of *bcl-2* in the *Irs2*$^{-/-}$ mice. A, mRNA expression levels in the islets of the wild-type and *Irs2*$^{-/-}$ mice after 20 wk of vildagliptin treatment by real-time PCR (n = 5); B, *upper panel*, protein expression of Bcl-2, Bax, cleaved caspase-3, caspase-3, and glyceraldehyde-3-phosphate dehydrogenase (GAPDH) in the islets of the wild-type and Irs2$^{-/-}$ mice after 20 wk of vildagliptin treatment by Western blotting; *lower panel*, intensity of the signals quantified by densitometry (NIH ImageJ) and corrected by the intensity of the GAPDH signal (n = 3). *, $P < 0.05$. The results are presented as the mean ± SE.

previously hypothesized that Irs2 is involved not only in β-cell proliferation but also in protecting against apoptosis (7–9). Here, we examined the effect of 20 wk vildagliptin treatment on the glucose tolerance and β-cell mass in wild-type, $Irs2^{+/-}$, and $Irs2^{-/-}$ mice fed a HF diet. We confirmed the effect of vildagliptin on the β-cell mass *in vivo* and demonstrated two novel findings. First, long-term administration of vildagliptin improved the glucose metabolism in the $Irs2^{+/-}$ and $Irs2^{-/-}$ mice fed a HF diet. Second, and more importantly, vildagliptin had the potential to reduce β-cell apoptosis in an Irs2-independent manner in the $Irs2^{-/-}$ mice.

The results of this study showed that vildagliptin administered for 20 wk had a glucose-lowering efficacy. It has been reported that vildagliptin treatment for 12 wk improved the glucose tolerance in rodents (18). On the other hand, we demonstrated its effect of longer-term treatment. Thus, vildagliptin is able to improve glucose metabolism over the long term even under HF diet-fed conditions, although whether long-term treatment *per se* might affect the glucose tolerance is not known. The changes observed in the OGTT performed 1 d after discontinuation of vildagliptin administration demonstrated that vildagliptin still exerted a glucose-lowering efficacy in addition to its direct effects in the $Irs2^{+/-}$ and $Irs2^{-/-}$ mice. But in the wild-type mice, such efficacy was not observed in the OGTT performed 1 d after discontinuation of vildagliptin administration. Taken together with the results on the roles of vildagliptin in β-cell function and β-cell mass, the effect of long-term administration of vildagliptin on glucose tolerance in the $Irs2^{-/-}$ mice seems to be attributable to the increased β-cell mass rather than to improved β-cell function, and the glucose-lowering efficacy in the wild-type mice in the OGTT seems to be mainly due to a direct effect of vildagliptin on insulin secretion.

The results of this study also demonstrated that vildagliptin increased the β-cell mass in the $Irs2^{-/-}$ mice by protecting the cells against apoptosis, rather than by stimulating their proliferation. This result raises the possibility that vildagliptin might suppress β-cell apoptosis in an Irs2-independent manner in the $Irs2^{-/-}$ mice. Because it has previously been reported that GLP-1 receptor agonists stimulated β-cell proliferation and neogenesis and inhibited β-cell apoptosis, thereby increasing the β-cell mass in rodents (11, 27), and that a GLP-1 receptor agonist failed to increase the β-cell mass and proliferation in $Irs2^{-/-}$ mice (12), Irs2 is thought to be required for GLP-1 signaling to increase the β-cell mass. These results prompted us to hypothesize that vildagliptin might increase the β-cell mass in wild-type mice but not in $Irs2^{-/-}$ mice; therefore, our findings were unexpected.

Park *et al.* (12) supposed the inhibition of apoptosis by exendin-4 largely failed in the $Irs2^{-/-}$ mice because the β-cell mass in these mice decreased to a similar degree as that in the $Irs2^{-/-}$ islets, irrespective of whether or not the mice were treated with exendin-4. By contrast, we here demonstrated that vildagliptin increased the β-cell mass by reducing β-cell apoptosis in the $Irs2^{-/-}$ mice. However, there were some environmental differences between our study and the previously cited study. First, the genetic background of our $Irs2^{-/-}$ mice was different from that of their $Irs2^{-/-}$ mice, which showed utterly damaged β-cells. Second, we treated the mice with a DPP-4 inhibitor for 20 wk, and they treated mice with a GLP-1 receptor agonist for 4 wk. Taken together, it seems likely that vildagliptin may have the potential to suppress β-cell apoptosis by both Irs2-dependent and Irs-2-independent pathways in $Irs2^{-/-}$ mice.

What then is the Irs2-independent pathway? The binding of GLP-1 to its specific receptor on the pancreatic β-cells leads to activation of adenylate cyclase activity and production of cAMP (28). Xie *et al.* (29) reported that mice with β-cell-specific Gsα deficiency showed significantly increased β-cell apoptosis, whereas expression of *Irs2* and the downstream *Pdx1* gene remained unaffected. Kim *et al.* (30) also reported that stimulation of INS-1 cells with GIP resulted in increased Bcl-2 promoter activity involving cAMP/protein kinase A-dependent regulation of cAMP response element-binding protein (CREB) activity, which seems to play an important role in the survival of β cells (31). In the present study, vildagliptin increased the mRNA expression level of *bcl-2* in the $Irs2^{-/-}$ mice, but such alteration was not evident in the protein levels (Fig. 6, A and B). We therefore assume that it is uncertain whether the increased *bcl-2* mRNA expression was involved in the Irs2-independent antiapoptotic effect of vildagliptin through the cAMP/protein kinase A/CREB protein pathway. Further study is needed to clarify the detailed molecular mechanisms.

In general, DPP-4 inhibitors behave as secretagogues and improve β-cell function, as a direct effect, in adult rodents (26, 32). In addition, DPP-4 inhibitors have the potential to induce long-term increase of the β-cell mass, which is attributed to its activity of increasing the proliferative activity and decreasing the apoptotic activity of the β-cells (19, 23). Moreover, the results of the current study revealed that vildagliptin could suppress β-cell apoptosis even in the absence of Irs2.

In summary, chronic administration of vildagliptin in $Irs2^{-/-}$ mice improved the glucose metabolism and suppressed β-cell apoptosis. These findings suggest that vildagliptin may be extremely promising for the treatment of diabetes mellitus.

Acknowledgments

We thank Mitsuyo Kaji and Eri Sakamoto for their excellent technical assistance and animal care and Misa Katayama for her secretarial assistance. We also thank Novartis Pharmaceuticals Co. (East Hanover, NJ) for providing the vildagliptin (LAF237) and encouraging this research.

Address all correspondence and requests for reprints to: Yasuo Terauchi, M.D., Ph.D., Professor, Department of Endocrinology and Metabolism, Graduate School of Medicine, Yokohama City University, 3-9 Fukuura, Kanazawa-ku, Yokohama 236-0004, Japan. E-mail: terauchi-tky@umin.ac.jp.

This work was supported in part by a Grant-in-Aid for Scientific Research (B) 19390251 and (B) 21390282 from the Ministry of Education, Culture, Sports, Science, and Technology (MEXT) of Japan, a Medical Award from the Japan Medical Association, a Grant-in-Aid from the Japan Diabetes Foundation, a Grant-in-Aid from the Suzuken Memorial Foundation, a Grant-in-Aid from the Naito Foundation, and a Grant-in-Aid from the Uehara Memorial Foundation (to Y.T.).

Disclosure Summary: K.S., A.N., J.S., T.M., Y.T., K.S., K.O., N.K., and T.K. have nothing to declare.

References

1. **Taylor SI, Accili D, Imai Y** 1994 Insulin resistance or insulin deficiency. Diabetes 43:735–740
2. **Polonsky KS, Sturis J, Bell GI** 1996 Non-insulin-dependent diabetes mellitus: a genetically programmed failure of the β-cell to compensate for insulin resistance. N Engl J Med 334:777–783
3. **Prentki M, Nolan CJ** 2006 Islet β-cell failure in type 2 diabetes. J Clin Invest 116:1802–1812
4. **Butler AE, Janson J, Bonner-Weir S, Ritzel R, Rizza RA, Butler PC** 2003 β-Cell deficit and increased β-cell apoptosis in humans with type 2 diabetes. Diabetes 52:102–110
5. **White MF** 1998 The IRS-signalling system: a network of docking proteins that mediate insulin action. Mol Cell Biochem 182:3–11
6. **Kubota N, Tobe K, Terauchi Y, Eto K, Yamauchi T, Suzuki R, Tsubamoto Y, Komeda K, Nakano R, Miki H, Satoh S, Sekihara H, Sciacchitano S, Lesniak M, Aizawa S, Nagai R, Kimura S, Akanuma Y, Taylor SI, Kadowaki T** 2000 Disruption of insulin receptor substrate 2 causes type 2 diabetes because of liver insulin resistance and lack of compensatory β-cell hyperplasia. Diabetes 49:1880–1889
7. **Terauchi Y, Takamoto I, Kubota N, Matsui J, Suzuki R, Komeda K, Hara A, Toyoda Y, Miwa I, Aizawa S, Tsutsumi S, Tsubamoto Y, Hashimoto S, Eto K, Nakamura A, Noda M, Tobe K, Aburatani H, Nagai R, Kadowaki T** 2007 Glucokinase and IRS-2 are required for compensatory β-cell hyperplasia in response to high-fat diet-induced insulin resistance. J Clin Invest 117:246–257
8. **Withers DJ, Burks DJ, Towery HH, Altamuro SL, Flint CL, White MF** 1999 Irs-2 coordinates Igf-1 receptor-mediated β-cell development and peripheral insulin signaling. Nat Genet 23:32–40
9. **Li D, Yin X, Zmuda EJ, Wolford CC, Dong X, White MF, Hai T** 2008 The repression of IRS2 gene by ATF3, a stress-inducible gene, contributes to pancreatic β-cell apoptosis. Diabetes 57:635–644
10. **Drucker DJ** 2006 The biology of incretin hormones. Cell Metab 3:153–165
11. **Farilla L, Hui H, Bertolotto C, Kang E, Bulotta A, Di Mario U, Perfetti R** 2002 Glucagon-like peptide-1 promotes islet cell growth and inhibits apoptosis in Zucker diabetic rats. Endocrinology 143:4397–4408
12. **Park S, Dong X, Fisher TL, Dunn S, Omer AK, Weir G, White MF** 2006 Exendin-4 uses Irs2 signaling to mediate pancreatic β-cell growth and function. J Biol Chem 281:1159–1168
13. **Deacon CF, Nauck MA, Toft-Nielsen M, Pridal L, Willms B, Holst JJ** 1995 Both subcutaneously and intravenously administered glucagon-like peptide I are rapidly degraded from the NH_2-terminus in type II diabetic patients and in healthy subjects. Diabetes 44:1126–1131
14. **Kieffer TJ, McIntosh CH, Pederson RA** 1995 Degradation of glucose-dependent insulinotropic polypeptide and truncated glucagon-like peptide 1 *in vitro* and *in vivo* by dipeptidyl peptidase IV. Endocrinology 136:3585–3596
15. **Winzell MS, Ahrén B** 2004 The high-fat diet-fed mouse: A model for studying mechanisms and treatment of impaired glucose tolerance and type 2 diabetes. Diabetes 53:S215–S219
16. **Flock G, Baggio LL, Longuet C, Drucker DJ** 2007 Incretin receptors for glucagon-like peptide 1 and glucose-dependent insulinotropic polypeptide are essential for the sustained metabolic actions of vildagliptin in mice. Diabetes 56:3006–3013
17. **Ahrén B, Winzell MS, Wierup N, Sundler F, Burkey B, Hughes TE** 2007 DPP-4 inhibition improves glucose tolerance and increases insulin and GLP-1 responses to gastric glucose in association with normalized islet topography in mice with β-cell-specific overexpression of human islet amyloid polypeptide. Regul Pept 143:97–103
18. **Raun K, von Voss P, Gotfredsen CF, Golozoubova V, Rolin B, Knudsen LB** 2007 Liraglutide, a long-acting glucagon-like peptide-1 analog, reduces body weight and food intake in obese candy-fed rats, whereas a dipeptidyl peptidase-IV inhibitor, vildagliptin, does not. Diabetes 56:8–15
19. **Cheng Q, Law PK, de Gasparo M, Leung PS** 2008 Combination of the dipeptidyl peptidase IV inhibitor LAF237 with the angiotensin II type 1 receptor antagonist valsartan enhances pancreatic islet morphology and function in a mouse model of type 2 diabetes. J Pharmacol Exp Ther 327:683–691
20. **Duttaroy A, Voelker F, Merriam K, Zhang X, Ren X, Subramanian K, Hughes TE, Burkey BF** 2011 The DPP-4 inhibitor vildagliptin increases pancreatic β-cell mass in neonatal rats. Eur J Pharmacol 650:703–707
21. **Nakamura A, Terauchi Y, Ohyama S, Kubota J, Shimazaki H, Nambu T, Takamoto I, Kubota N, Eiki J, Yoshioka N, Kadowaki T, Koike T** 2009 Impact of small-molecule glucokinase activator on glucose metabolism and β-cell mass. Endocrinology 150:1147–1154
22. **Ahrén B, Winzell MS, Burkey B, Hughes TE** 2005 β-Cell expression of a dominant-negative HNF-1α compromises the ability of inhibition of dipeptidyl peptidase-4 to elicit a long-term augmentation of insulin secretion in mice. Eur J Pharmacol 521:164–168
23. **Shirakawa J, Amo K, Ohminami H, Orime K, Togashi Y, Ito Y, Tajima K, Koganei M, Sasaki H, Takeda E, Terauchi Y** 2011 Protective effect of dipeptidyl peptidase-4 (DPP-4) inhibitor against increased β-cell apoptosis induced by dietary sucrose and linoleic acid in mice with diabetes. J Biol Chem 286:25467–25476
24. **Eto K, Tsubamoto Y, Terauchi Y, Sugiyama T, Kishimoto T, Takahashi N, Yamauchi N, Kubota N, Murayama S, Aizawa T, Akanuma Y, Aizawa S, Kasai H, Yazaki Y, Kadowaki T** 1999 Role of NADH shuttle system in glucose-induced activation of mitochondrial metabolism and insulin secretion. Science 283:981–985
25. **Mu J, Petrov A, Eiermann GJ, Woods J, Zhou YP, Li Z, Zycband E, Feng Y, Zhu L, Roy RS, Howard AD, Li C, Thornberry NA, Zhang BB** 2009 Inhibition of DPP-4 with sitagliptin improves glycemic control and restores islet cell mass and function in a rodent model of type 2 diabetes. Eur J Pharmacol 623:148–154
26. **Zhang X, Wang Z, Huang Y, Wang J** 2011 Effects of chronic administration of alogliptin on the development of diabetes and β-cell

function in high fat diet/streptozotocin diabetic mice. Diabetes Obes Metab 13:337–347
27. **Jhala US, Canettieri G, Screaton RA, Kulkarni RN, Krajewski S, Reed J, Walker J, Lin X, White M, Montminy M** 2003 cAMP promotes pancreatic β-cell survival via CREB-mediated induction of IRS2. Genes Dev 17:1575–1580
28. **Sloop KW, Willard FS, Brenner MB, Ficorilli J, Valasek K, Showalter AD, Farb TB, Cao JX, Cox AL, Michael MD, Gutierrez Sanfeliciano SM, Tebbe MJ, Coghlan MJ** 2010 Novel small molecule glucagon-like peptide-1 receptor agonist stimulates insulin secretion in rodents and from human islets. Diabetes 59:3099–3107
29. **Xie T, Chen M, Zhang QH, Ma Z, Weinstein LS** 2007 β-cell-specific deficiency of the stimulatory G protein α-subunit Gsα leads to reduced β-cell mass and insulin-deficient diabetes. Proc Natl Acad Sci USA 104:19601–19606
30. **Kim SJ, Nian C, Widenmaier S, McIntosh CHS** 2008 Glucose-dependent insulinotropic polypeptide-mediated up-regulation of β-cell antiapoptotic Bcl-2 gene expression is coordinated by cyclic AMP response element binding protein and cAMP-responsive CREB coactivator 2. Mol Cell Biol 28:1644–1656
31. **Jambal P, Masterson S, Nesterova A, Bouchard R, Bergman B, Hutton JC, Boxer LM, Reusch JE, Pugazhenthi S** 2003 Cytokine-mediated down-regulation of the transcription factor cAMP-response element-binding protein in pancreatic β-cells. J Biol Chem 278: 23055–23065
32. **Mu J, Woods J, Zhou YP, Roy RS, Li Z, Zycband E, Feng Y, Zhu L, Li C, Howard AD, Moller DE, Thornberry NA, Zhang BB** 2006 Chronic inhibition of dipeptidyl peptidase-4 with a sitagliptin analog preserves pancreatic β-cell mass and function in a rodent model of type 2 diabetes. Diabetes 55:1695–1704

SnapShot: Physiology of Insulin Signaling

Takashi Kadowaki, Naoto Kubota, Kohjiro Ueki, and Toshimasa Yamauchi
Department of Diabetes and Metabolic Diseases, Graduate School of Medicine, University of Tokyo, Bunkyo-ku, Tokyo 113-8655, Japan

	CELL TYPE/ ORGAN	PROTEIN	LOSS OF FUNCTION PHENOTYPES
MOUSE (KNOCKOUT)	**Systemic**	IR	Apparently normal intrauterine growth and development, severe hyperglycemia and hyperketonemia, perinatal death as the result of diabetic ketoacidosis within 48–72 hours
		IRS-1	Retarded embryonal and postnatal growth, insulin resistance, normal fasting glycemia and normal or mild glucose intolerance, hyperinsulinemia
		IRS-2	Insulin resistance, impaired glucose tolerance, impaired insulin secretion, decreased β cell mass
	Brain	IR	*Obesity, increased body fat mass, insulin resistance, hyperinsulinemia, hypertriglyceridemia,* increased food intake (female only)
		IRS-2	Obesity, increased body fat mass, insulin resistance, impaired glucose tolerance, hyperinsulinemia, extended life span, more active and greater glucose oxidation, increased superoxide dismutase-2 in the hypothalamus
	Liver	IR	Normal body weight, severe insulin resistance, impaired glucose tolerance, hyperinsulinemia, increased hepatic glucose production
		IRS-1	Normal body weight, normal insulin sensitivity during fasting but insulin resistance after refeeding
		IRS-2	Normal body weight, normal insulin sensitivity after refeeding but insulin resistance during fasting
		IRS-1/IRS-2	Normal body weight, severe insulin resistance, severe glucose intolerance, marked hyperinsulinemia
	Skeletal muscle	IR	Normal body weight, normal insulin and glucose tolerance, increased epididymal fat pad, hypertriglyceridemia, increased FFA levels
		IRS-1	Normal body weight, normal insulin and glucose tolerance, decreased skeletal muscle mass
		IRS-2	Normal body weight, normal insulin and glucose tolerance, normal skeletal muscle mass
		IRS-1/IRS-2	Reduced body weight and body length, insulin resistance, normal glucose tolerance, reduced skeletal muscle mass, increased lactate levels
	Heart	IR	Normal body weight, normal insulin and glucose tolerance, decreased cardiac size and cardiac output, decreased fatty acid oxidation
	Kidney	IR	Normal body weight, normal insulin and glucose tolerance, albuminuria, histological features of diabetic nephropathy
	β cell	IR	Normal body weight, normal insulin tolerance, impaired glucose tolerance, impaired glucose-stimulated insulin secretion, decreased β cell mass
		IRS-2	Impaired glucose tolerance, impaired insulin secretion, decreased β cell mass
	Macrophage	IR	Normal body weight, normal insulin and glucose tolerance, protected from obesity-linked insulin resistance due to decreased hepatic glucose production and increased glucose disposal in skeletal muscle
	Endothelial cell	IR	Normal body weight, normal insulin and glucose tolerance, reduced eNOS and endothelin-1 expression, insulin resistance on a low-salt diet
		IRS-1	Normal body weight, normal insulin and glucose tolerance, normal insulin signaling in endothelial cells
		IRS-2	Normal body weight, insulin resistance, impaired glucose tolerance, impaired insulin-induced eNOS phosphorylation, attenuation of insulin-induced capillary recruitment and insulin delivery associated with reduced glucose uptake by skeletal muscle
		IRS-1/IRS-2	Normal body weight, insulin resistance, impaired glucose tolerance, impaired insulin-induced eNOS phosphorylation in endothelial cells
	Adipose tissue	IR	Reduced body weight and fat mass, protected from Gold thioglucose (GTG)-induced obesity, insulin resistance, impared glucose tolerance, extended life span
HUMAN	**Systemic**	IR mutation	Hyperglycemia, hyperinsulinemia, severe insulin resistance, acanthosis nigricans, hyperandrogenemia

See online version for legend and references.

SnapShot: Physiology of Insulin Signaling

Takashi Kadowaki, Naoto Kubota, Kohjiro Ueki, and Toshimasa Yamauchi
Department of Diabetes and Metabolic Diseases, Graduate School of Medicine, University of Tokyo, Bunkyo-ku, Tokyo 113-8655, Japan

Many facets of metabolic syndrome arise from changes in insulin sensitivity and the downstream signaling responses. Mouse models have provided useful tools for studying and understanding the mechanisms underlying the human disease phenotypes. Insulin signaling relies on activation of the insulin receptor (IR) and subsequent phosphorylation of insulin receptor substrates (IRS), particularly IRS-1 and IRS-2. This SnapShot provides a guide to the mouse phenotypes resulting from knockout of IR, IRS-1, IRS-2, or IRS-1 and IRS-2 in different tissues and cell types. These phenotypes illustrate that IRS-1 and IRS-2 only show partial functional overlap. The systemic consequences of human mutations in IR are included and show highly related phenotypic outcomes.

REFERENCES

Biddinger, S.B., and Kahn, C.R. (2006). From mice to men: insights into the insulin resistance syndromes. Annu. Rev. Physiol. *68*, 123–158.

Blüher, M., Kahn, B.B., and Kahn, C.R. (2003). Extended longevity in mice lacking the insulin receptor in adipose tissue. Science *299*, 572–574.

Brüning, J.C., Gautam, D., Burks, D.J., Gillette, J., Schubert, M., Orban, P.C., Klein, R., Krone, W., Müller-Wieland, D., and Kahn, C.R. (2000). Role of brain insulin receptor in control of body weight and reproduction. Science *289*, 2122–2125.

Dong, X.C., Copps, K.D., Guo, S., Li, Y., Kollipara, R., DePinho, R.A., and White, M.F. (2008). Inactivation of hepatic Foxo1 by insulin signaling is required for adaptive nutrient homeostasis and endocrine growth regulation. Cell Metab. *8*, 65–76.

Kadowaki, T., Bevins, C.L., Cama, A., Ojamaa, K., Marcus-Samuels, B., Kadowaki, H., Beitz, L., McKeon, C., and Taylor, S.I. (1988). Two mutant alleles of the insulin receptor gene in a patient with extreme insulin resistance. Science *240*, 787–790.

Kadowaki, T., Ueki. K., Yamauchi, T., and Kubota N. (2012). SnapShot: Insulin signaling pathways. Cell *148*, 624–624.e1.

Kubota, N., Kubota, T., Itoh, S., Kumagai, H., Kozono, H., Takamoto, I., Mineyama, T., Ogata, H., Tokuyama, K., Ohsugi, M., et al. (2008). Dynamic functional relay between insulin receptor substrate 1 and 2 in hepatic insulin signaling during fasting and feeding. Cell Metab. *8*, 49–64.

Kubota, T., Kubota, N., Kumagai, H., Yamaguchi, S., Kozono, H., Takahashi, T., Inoue, M., Itoh, S., Takamoto, I., Sasako, T., et al. (2011). Impaired insulin signaling in endothelial cells reduces insulin-induced glucose uptake by skeletal muscle. Cell Metab. *13*, 294–307.

Kulkarni, R.N., Brüning, J.C., Winnay, J.N., Postic, C., Magnuson, M.A., and Kahn, C.R. (1999). Tissue-specific knockout of the insulin receptor in pancreatic beta cells creates an insulin secretory defect similar to that in type 2 diabetes. Cell *96*, 329–339.

Taguchi, A., Wartschow, L.M., and White, M.F. (2007). Brain IRS2 signaling coordinates life span and nutrient homeostasis. Science *317*, 369–372.

  DOI 10.1016/j.cell.2012.02.004